

On the Role of the Corner Radius in the Mechanical Behavior of the Hexagonal
Honeycomb

by

Athul Rajeev

A Thesis Presented in Partial Fulfillment
of the Requirements for the Degree
Master of Science

Approved June 2021 by the
Graduate Supervisory Committee:

Dhruv Bhate, Chair
Jay Oswald
Hamidreza Marvi

ARIZONA STATE UNIVERSITY

August 2021

ABSTRACT

The hexagonal honeycomb is a bio-inspired cellular structure with a high stiffness-to-weight ratio. It has contributed to its use in several engineering applications compared to solid bodies with identical volume and material properties. This characteristic behavior is mainly attributed to the effective nature of stress distribution through the honeycomb beams that manifests as bending, axial, and shear deformation mechanisms. Inspired by the presence of this feature in natural honeycomb, this work focuses on the influence of the corner radius on the mechanical properties of a honeycomb structure subjected to in-plane compression loading. First, the local response at the corner node interface is investigated with the help of finite element simulation of a periodic unit cell within the linear elastic domain and validated against the best available analytical models. Next, a parametric design of experiments (DOE) study with the unit cell is defined with design points of varying circularity and cell length ratios towards identifying the optimal combination of all geometric parameters that maximize stiffness per unit mass while minimizing the stresses induced at the corner nodes. The observed trends are then compared with compression tests of 3D printed Nylon 12 honeycomb specimens of varying corner radii and wall thicknesses. The study concluded that the presence of a corner radius has a mitigating effect on peak stresses but that these effects are dependent on thickness while also increasing specific stiffness in all cases. It also points towards an optimum combination of parameters that achieve both objectives simultaneously while shedding some light on the functional benefit of this radius in wasp and bee nests that employ a hexagonal cell.

ACKNOWLEDGMENTS

I want to thank Varun Agrawal for laying the foundation of the parametric micromechanical approach and the valuable tips and insights to improve the honeycomb unit cell study further. Special thanks to Mandar Shinde for training me to use the INSTRON 5985 mechanical testing machine, helping me identify potential problems in my numerical analysis, and help me understand the usage of different beam theories and finite element types. Additional thanks to Irving Ramirez for guiding me to use the INSTRON machine safely to conduct compression tests and tips to capture the test video footage efficiently, Prince Lazar for guidance on validating the Nylon 12 plasticity model, and Cameron Noe for his efforts in SLS 3D printing the honeycomb specimens and for the training provided to post-process the honeycomb specimens. I am grateful to Dr.Dhruv Bhate, thesis advisor and committee chair, for giving me the opportunity to work on this research topic and for the immense guidance and commitment to complete the research work. Finally, I want to thank my parents for their support and love towards my well-being and interests.

TABLE OF CONTENTS

	Page
LIST OF TABLES	v
LIST OF FIGURES	vi
CHAPTER	
1 INTRODUCTION	1
Background.....	1
Research Questions.....	4
Research Objectives	4
Literature on Honeycomb Mechanics.....	5
2 FINITE ELEMENT MODEL DEVELOPMENT AND VALIDATION	9
Parametric Unit Cell Design	9
Finite Element Model Setup.....	10
Mesh Refinement Study	13
Numerical Model Validation Study	15
3 PARAMETRIC DESIGN STUDY	19
Mechanical Response Plots.....	22
Response Surface Plots	27
4 EXPERIMENTAL STUDY	30
Honeycomb Specimen Design.....	30
Manufacturing and Characterization.....	32
Compression Test Methodology	38
Compression Test Results	39

CHAPTER	Page
5 ANALYSIS AND DISCUSSION	45
Comparing Trends Between Numerical and Experimental Data.....	45
6 CONCLUSION	51
Future Work.....	53
REFERENCES	54
APPENDIX	
A NYLON 12 MATERIAL MODEL	57

LIST OF TABLES

Table	Page
1. DOE Design Table	19
2. RSM Design Table	27
3. Specimen Design Table	31
4. Comparision Between Measured and Actual t/l And r_o/r Ratios	37

LIST OF FIGURES

Figure	Page
1. Hexagonal Honeycomb Subjected to In-plane Loading (L. J. Gibson)	1
2. Plateau Border or Corner Radii at the Junction of Naturally occurring Honeycomb (D. Goss et al.)	2
3. Average Corner Radius against Cell Diameter in Honeybee Nests (D. Goss et al.)	3
4. Commercial Aluminum Honeycomb Designations.....	4
5. In-plane Stress-Strain Behavior of Honeycomb with Initial Linear Elastic Region followed by Plastic Plateau and Densification (J. A. Naim)	5
6. Bending Deformation Mechanism under In-Plane Loading for X1(left) and X2 (right) Directions (L.J. Gibson)	6
7. In-Plane Shearing Deformation Mechanism (S. Malek)	7
8. Plateau Border Model (Chuang)	7
9. Comparision of Different Models without Corner Radius	8
10. Python Script to Parametrically Design Honeycomb Unit Cell.....	9
11. Honeycomb RVE	10
12. Numerical Model Setup – Boundary Conditions and Constraint Equations	11
13. In-Plane Elastic Moduli Calculaitons	12
14. Numerical Model - Unit cell Meshing Constraints	13
15. In-Plane Elastic Moduli Mesh Convergence Study.....	14

Figure	Page
16. Comparing In-plane Elastic Modulus of a Numerical Model with Malek & Gibson Analytical Model	15
17. Updated Numerical Model Elastic Moduli Properties Plot with Rigid Triangular Nodal Assumption against the Analytical Model	16
18. Nodal Deformation with Increment in t/l Ratio.....	17
19. Numerical Model vs. Chuang-Huang Plateau Border Model	18
20. Corner Radius Stress Evaluation Path	20
21. Honeycomb Unit Cells with varying Geometric Parameters (All units in mm)	21
22. Geometric Efficiency vs. Normalised Max Corner Stress	22
23. Onset of Plasticity with Varying t/l and r_c/r ratios.....	23
24. Variation of Max Corner Stress with Circularity (Linear-Elastic).....	24
25. Variation of Max Corner Stress with Circularity (Elastic-plastic).....	25
26. Variation of a Max Plastic Strain with Circularity (Elastic-plastic)	25
27. Evolution of Stress Distribution of Unit Cell with increasing circularity....	26
28. RSM plot of Geometric Efficiency varied with t/l ratio and r_c/r ratio	28
29. RSM plot of Normalized Max Corner Stress varied with t/l ratio and r_c/r ratio	29
30. Honeycomb Specimen Design (left) and Width Standard (right).....	30
31. SLS 3D Printing.....	32
32. Honeycomb Specimens arranged in the Build Chamber.....	33
33. Post-processing of Honeycomb Specimens.....	34

Figure	Page
34. Bead Blasting of the Specimen with Glass powder.....	34
35. Keyence VR-3200 Imager.....	35
36. Optical Measurements using Keyence Imager	36
37. Instron 5985 Universal Testing Machine (left) and Test Setup (right).....	38
38. Compression Testing Results for Honeycombs with High Wall Thickness....	39
39. Comparing the Deformation Behavior between Specimen 1 & 4 at different Strain Levels	40
40. Compression Testing Results for Honeycombs with Baseline Specimens (Fixed Circularity with Varying Wall Thickness).....	41
41. Comparing the Deformation Behavior between Baseline 1&3 at Different Strain Levels	42
42. Compression Testing Results for Honeycombs with Low Wall Thickness.....	43
43. Compression Testing Results for Honeycombs with Medium Wall Thickness	43
44. Elastic Buckling (left) and Plastic Yielding Deformation (Right).....	44
45. Comparing Experimental and Numerical trends	46
46. Comparing Experimental Data with Numerical Von Mises Stress Contours, Smooth Plateau	47

Figure	Page
47. Comparing Experimental Data with Von Mises Stress Contours, Rough Plateau	48
48. Rotational Stiffness vs. Bending Stiffness.....	49
49. Honeycomb Plateau Border with Triangular Node.....	50
50. Summary of In-plane Stress and Stiffness Characteristics.....	51
51. Paper Wasp Honeycomb Nests (D. Goss).....	53
52. 3D Lattice Structures with varying Beam Morphologies.....	53
53. Nylon 12 Tensile Test Setup.....	58
54. Nylon 12 True Stress-Strain plot at different Strain Rates.....	59
55. Multilinear Isotropic Hardening Plasticity model.....	59
56. Nylon 12 Dogbone Simulation.....	60
57. Force Displacement Comparison between Experimental and Numerical data	61
58. True Stress and Plastic Strain Comparison.....	62

CHAPTER 1

INTRODUCTION

1.1 Background

Cellular materials are derived from a combination of cells with varying orientations of solid edges conjoined together to form a repeating (periodic) or a non-repeating (aperiodic) cellular structure [1]. The hexagonal honeycomb is a periodic, prismatic bio-inspired cellular material that has been used for various engineering applications [2]. These structures have been studied numerically and experimentally for their mechanical responses and have been found to have high stiffness and strength per unit mass, and good energy-absorbing capabilities [3-7].

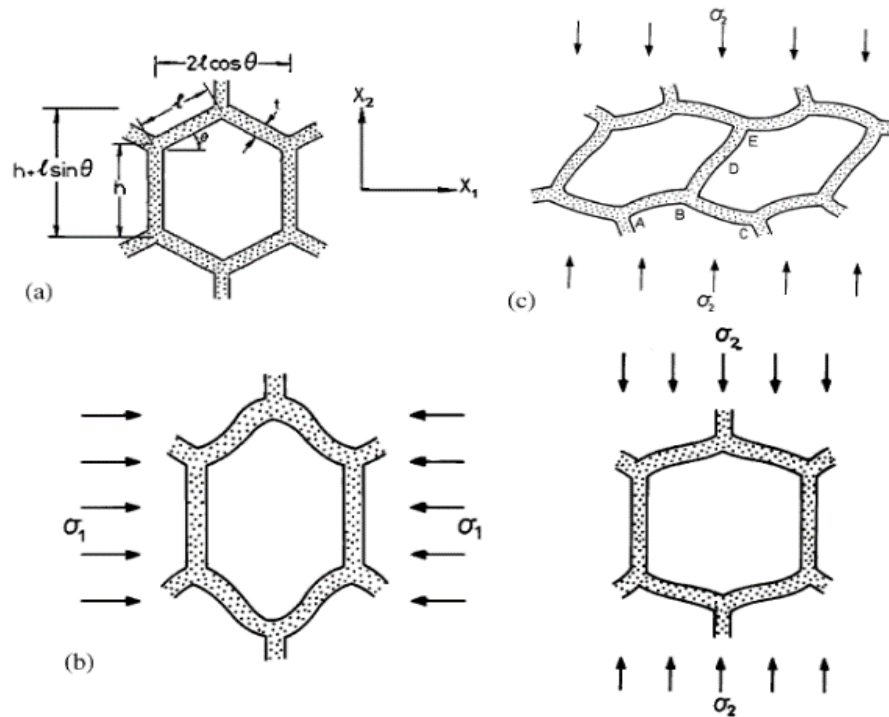


Figure 1: Hexagonal honeycomb subjected to In-plane loading (a) undeformed (b) linear elastic buckling (c) non-linear elastic buckling (L. J. Gibson)

Figure 1 represents a typical micro-mechanical approach to understand hexagonal honeycomb structures' mechanical behavior by discretizing it into repeating cells called Representative Volume Elements (RVE). This unit cell approach gives a good understanding of the local mechanical response and is helpful to analyze the optimum combination of geometric parameters to suit the mechanical requirements. Traditionally, honeycomb models have focused on the hexagonally arranged beams meeting at nodes with sharp corners. In recent studies, there is an increased emphasis on studying the mechanical properties of these cellular structures from a biological standpoint [8]. Studies [9-10] also indicate the presence of geometrical features such as corner radius in naturally occurring honeycombs at the nodal interface with the help of optical and X-ray visualization techniques. Karihaloo et al. [9] postulated that the bees initially make circular cells packed together like a layer of bubbles. The honeycomb wax is then softened by the heat generated by the bee's body temperature and then gets pulled into hexagonal cells by surface tension at the junctions where three walls meet. This leads to plateau borders or corner radii at the interface where the cell walls join together, as seen in Figure 2.

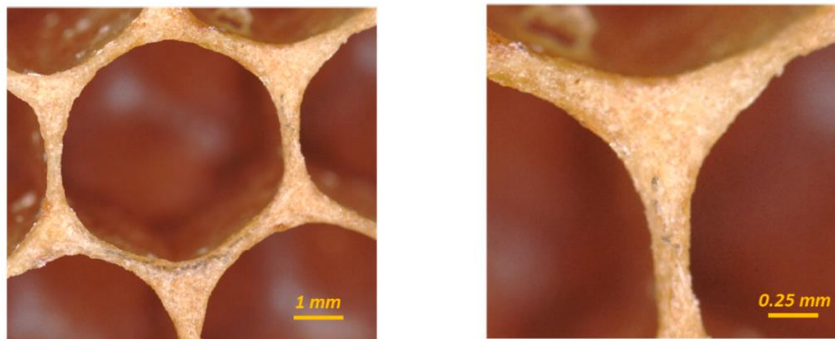


Figure 2: Plateau border or corner radii at the junction of naturally occurring honeycomb (D. Goss et al.)

A plot with the average corner radius measurements from six colonies of natural honeycomb nests (*A. mellifera*) considering the variation in corner radius and cell diameter for drone and worker cell is presented in Figure 3, which shows that honeybee nests have a very evident corner radius, and further that this corner radius increases with increasing cell size.

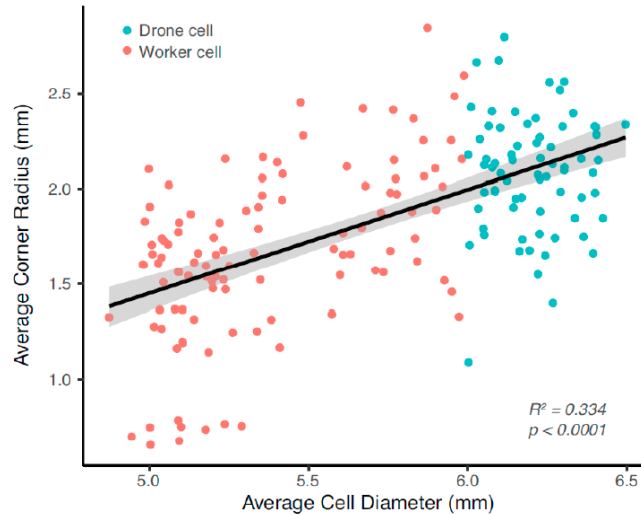


Figure 3: Average corner radius against cell diameter in honeybee nests (D. Goss et al.)

Goss et al. [10] studied the influence of these features on the mechanical properties when subjected to out-of-plane compression and 3-point bending honeycomb specimens fabricated with a 3D printing process called Selective Laser Sintering (SLS). The study concluded that a corner radius does not affect or improve specific stiffness (i.e., per unit mass) in out-of-plane compression but that the corner radius increases specific flexural strength under 3-point bending. Chuang et al. [11] showed that the elastic moduli and plastic collapse strength of honeycombs with low relative densities (volume fraction of material present in a cellular solid) and plateau borders (corner radii) depend on the volume fraction of solid present at the corner node.

1.2 Research Questions

From the above discussion, there is an opportunity to study the interaction between the various geometric features and optimize them for engineering applications. For example, major honeycomb panel manufacturers such as Hexcel characterize their commercial honeycombs with their material type, specification, cell size, and sheet size, as shown in Figure 4. In addition, most of the literature restricted their analysis to honeycombs with low relative densities, with little mention of the corner radius, primarily due to manufacturing limitations. Thus, the research question at the heart of this thesis is: ***How does the cell wall thickness and corner radius affect the stiffness and stress characteristics of a hexagonal honeycomb?*** A follow-on question is: ***What is the optimum combination of these parameters to maximize stiffness per unit mass while also reducing the peak stresses in the honeycomb?***

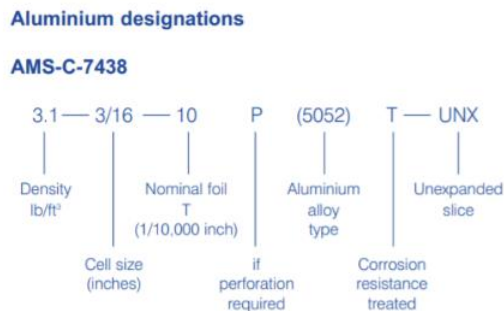


Figure 4: Commercial aluminum honeycomb designations

1.3 Research Objectives

The main objective of this research is to do a quantitative study of a hexagonal honeycomb at varying circularities and relative densities and identify a range of optimal parameters that will help maximize the stiffness and minimize stresses at the corner. This is accomplished with a numerical study of a honeycomb unit cell using finite element

analysis and comparing the observed deformation trends with in-plane compression tests of additively manufactured honeycomb specimens with varying geometric parameters such as the wall thickness, cell diameter, and corner radii.

1.4 Literature on honeycomb mechanics

Gibson et al. postulated that when a honeycomb unit cell is under in-plane compression, the cell walls first bend elastically. When the load reaches above critical peak stress, the cells collapse by elastic buckling, plastic yielding, creep, or brittle fracture, the specifics of which are a function of the composition of the material and the design parameters such as thickness and cell size. After the honeycomb cell collapses, the cell wall edges come into contact, causing it to close up and densify, illustrated as the stress-strain plot in Figure 5.

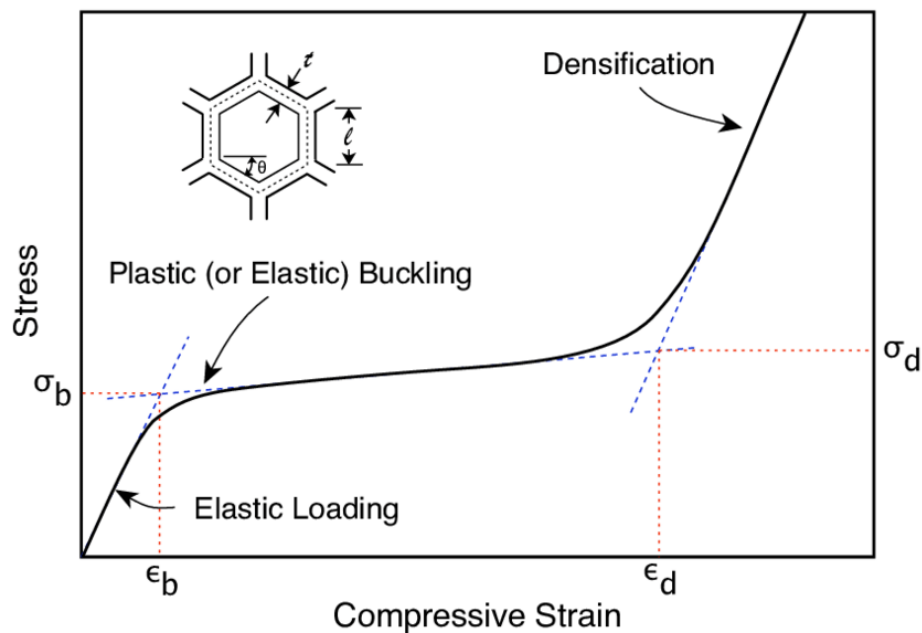


Figure 5: In-plane stress-strain behavior of honeycomb with initial linear elastic region followed by plastic plateau and densification (J. A. Naim)

The classical analytical model by Gibson describes the in-plane mechanical properties of a honeycomb unit cell. This model is derived using the Euler – Bernoulli beam bending theory and, in its simplest and most commonly used formulation, considers only the bending deformation mode. Figure 6 captures the bending deformation mechanism for the classical in-plane compression analytical model

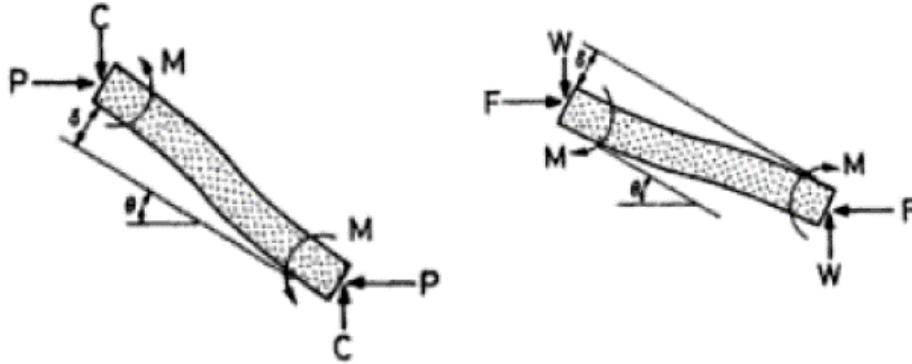


Figure 6: Bending deformation mechanism under in-plane loading for X1(left) and X2 (right) directions (L.J. Gibson)

Malek et al. [13] improved the classical Gibson & Ashby [1] model by considering the axial and shear deformation in the honeycomb beams and correcting the beam length associated with deformation (Figure 7). This model is derived using the Timoshenko beam theory [14], which postulates that the cross-section of a beam under bending does not remain perpendicular to the neutral surface. The Timoshenko model also captures the variation in the longitudinal strain and captures the deformation accurately for short and thick beams. Hence, this model is an excellent benchmark for any numerical study conducted to verify the accuracy of the mechanical properties of a hexagonal honeycomb.

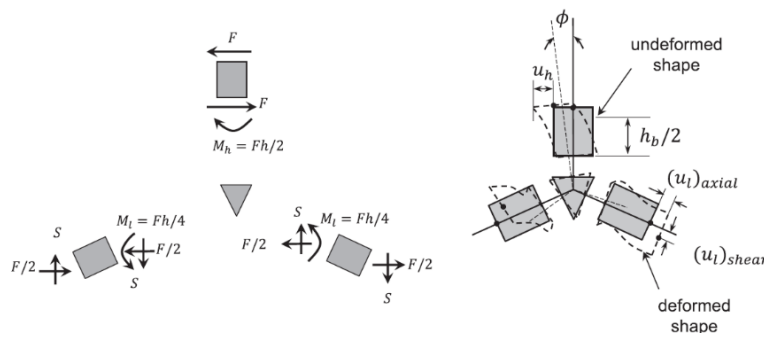
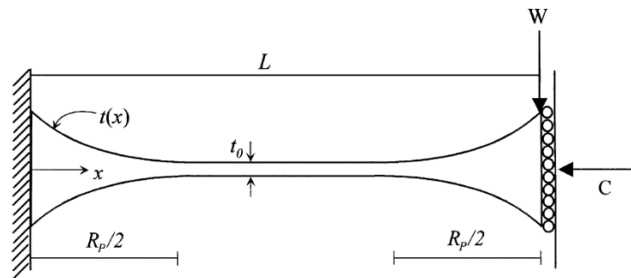
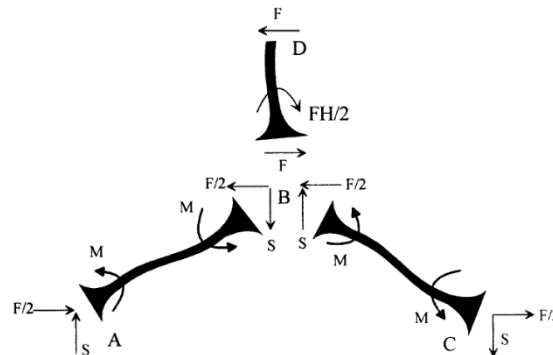


Figure 7: In-plane shearing deformation mechanism (S. Malek)

The analytical model developed by Malek et al. is, however, restricted to honeycombs without a corner radius. Chuang et al. developed analytical relationships that permit such a radius, by modeling honeycomb with plateau borders. This plateau border model discretizes the honeycomb cell wall into beams with variable thicknesses (Figure 8(a)). The analytical relationship was derived by considering the axial and bending deformation with the Euler-Bernoulli theory assumptions.



(a) Variable thickness beam model under axial and bending loads



(b) Load distribution of honeycombs with plateau borders

Figure 8: Plateau border model (Chuang)

In this work, the Malek and Gibson analytical model is used to verify the numerical model's periodicity and accuracy and validate the in-plane mechanical properties of the honeycomb and is limited to sharp-corner honeycombs only (i.e. without a corner radius). In contrast, the Huang and Chuang plateau border model is utilized as a baseline for the numerical model study with a corner radius. The predictions of specific stiffness (EI^*/E_s) against the thickness over cell length ratio (t/l) for the various honeycomb models available in the literature are graphically summarized in Figure 9, all shown for a honeycomb with no corner radius. EI^* represents the effective elastic modulus of the honeycomb, E_s represents the modulus of the honeycomb material composition. It can be seen that all models show good agreement at low t/l ratios but deviate from each other as t/l increases, primarily due to the increasing contributions of shear deformation (ignored in the Huang and Chuang model) and the increased stiffening of the honeycomb due to the shorter beam length assumptions in the Malek and Gibson model.

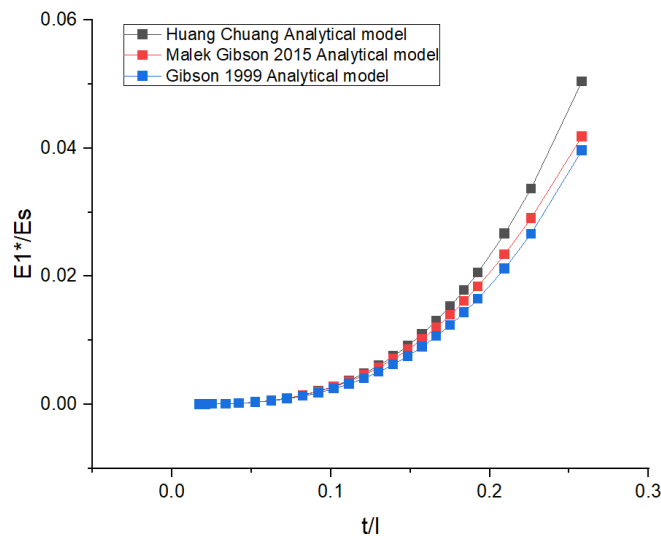


Figure 9: Comparison of different models without corner radius

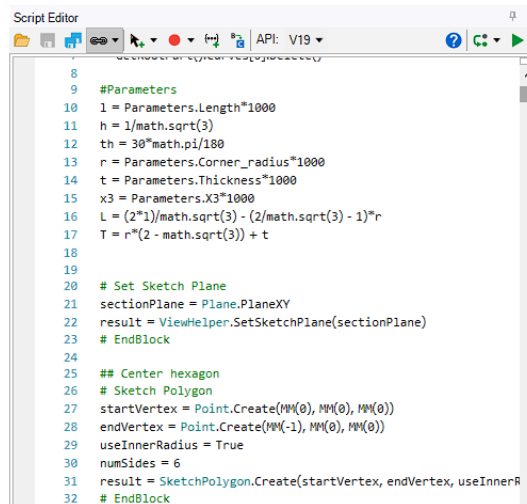
CHAPTER 2

FINITE ELEMENT MODEL DEVELOPMENT AND VALIDATION

The local mechanical response of the honeycomb structure may be analyzed by discretizing the honeycomb structure as a periodic repeating unit cell or Representative Volume Element (RVE). The available analytical models use this micromechanical approach to determine the in-plane mechanical properties [1,11,13]. Sorohan et al. [15] demonstrated using a repeating periodic unit cell for finite element analyses to extract honeycomb properties. The main benefit of the unit cell representation is the reduction in the computational effort required. The design, model setup, mesh refinement study, and validation against analytical models of the honeycomb RVE is discussed in the following sections.

2.1 Parametric Unit cell design

ANSYS SpaceClaim scripting feature was used to design the regular uniform honeycomb unit cell programmatically with a PYTHON-based script editor (Figure10).



```
Script Editor
8
9 #Parameters
10 l = Parameters.Length*1000
11 h = 1/math.sqrt(3)
12 th = 30*math.pi/180
13 r = Parameters.Corner_radius*1000
14 t = Parameters.Thickness*1000
15 x3 = Parameters.X3*1000
16 L = (2*1)/math.sqrt(3) - (2/math.sqrt(3) - 1)*r
17 T = r*(2 - math.sqrt(3)) + t
18
19
20 # Set Sketch Plane
21 sectionPlane = Plane.PlaneXY
22 result = ViewHelper.SetSketchPlane(sectionPlane)
23 # EndBlock
24
25 ## Center hexagon
26 # Sketch Polygon
27 startVertex = Point.Create(MM(0), MM(0), MM(0))
28 endVertex = Point.Create(MM(-1), MM(0), MM(0))
29 useInnerRadius = True
30 numSides = 6
31 result = SketchPolygon.Create(startVertex, endVertex, useInnerR
32 # EndBlock
```

Figure 10: Python script to parametrically design honeycomb unit cell

Cell diameter, corner radius, and wall thickness are varied design parameters within the python code. The honeycomb unit cell is divided into respective beams and triangular nodes to more precisely control the number of mesh elements across the beam using the imprinting feature in Spaceclaim seen in Figure 11.

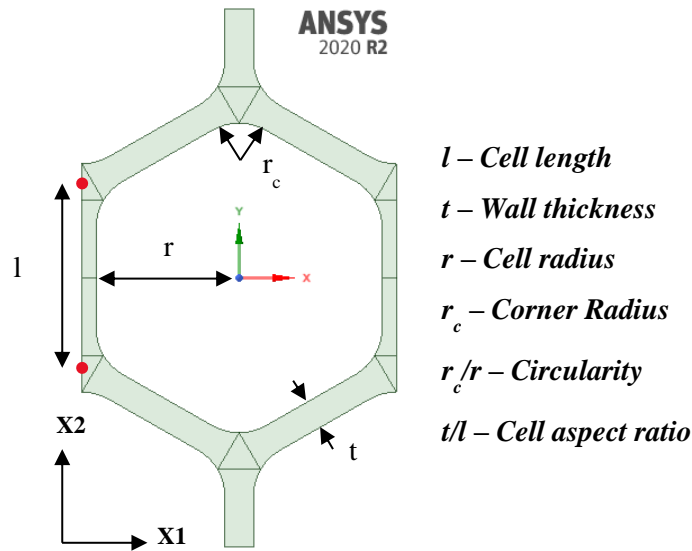
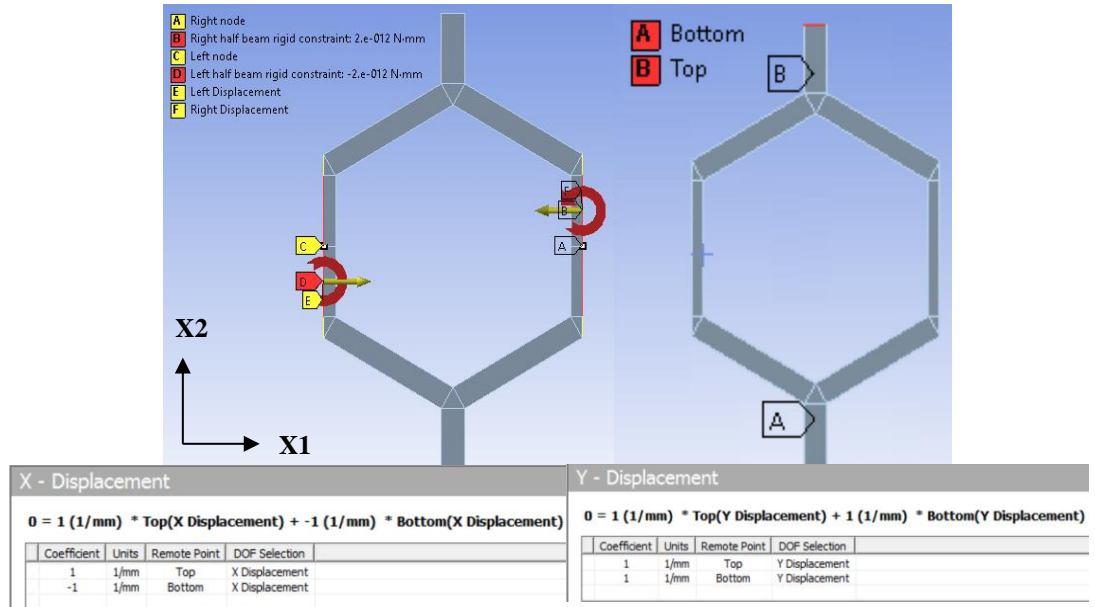


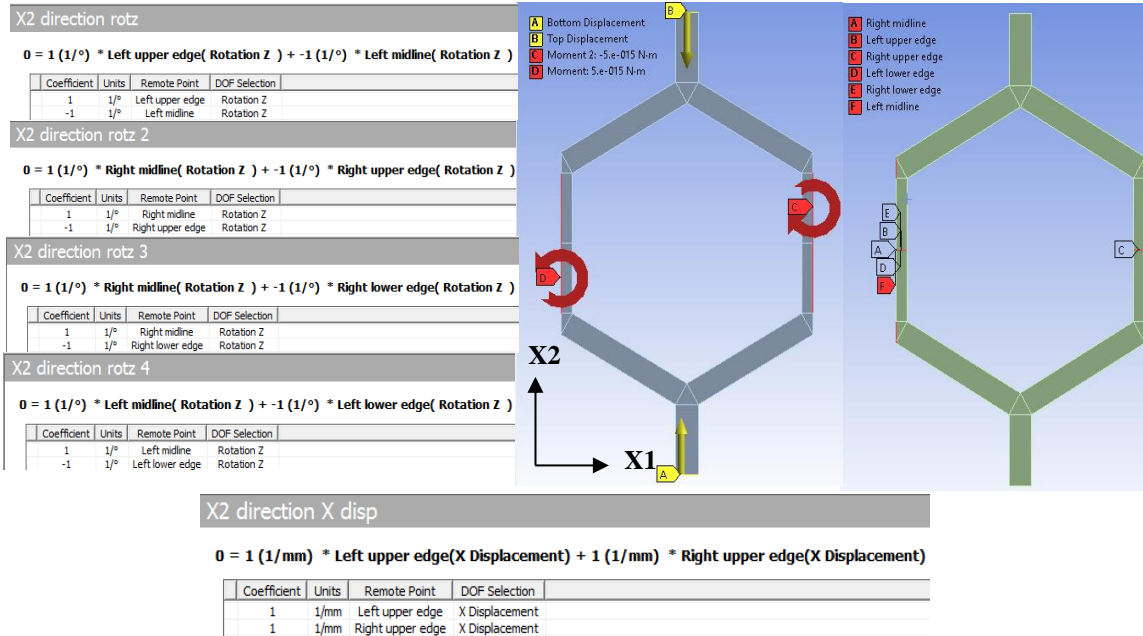
Figure 11: Honeycomb RVE

2.2 Numerical Model setup

A 2D planar numerical model of the honeycomb RVE with generalized plane strain conditions was developed for the X1 and X2 in-plane compression loading in ANSYS 2020 R2. The in-plane compression loading is defined with displacement boundary conditions applied on the cell boundary edges. The degrees of freedom of the unit cell is constrained with the help of remote points. In addition, the periodicity of the unit cell analysis is maintained by defining the edges on either side of the RVE, excluding the triangular node edges to be rigid with moment constraints. Figure 12 illustrates the model setup and constraint equations, respectively.



(a) X1 direction



(b) X2 direction

Figure 12: Numerical model setup – Boundary conditions and constraint equations

The in-plane elastic moduli in X1 and X2 directions are calculated from the reaction forces output probed from the applied displacements. For the 2D generalized plane strain model, the depth (b) of the unit cell remains constant for all simulations. The reaction forces output, cell dimensions, and numerical calculations are summarised in Figure 13, respectively. In the following section, the unit cell model is checked for convergence using an Isotropic material model [15] with Young's modulus of 1000 MPa, yield strength of 100 MPa, and Poisson's ratio of 0.3.

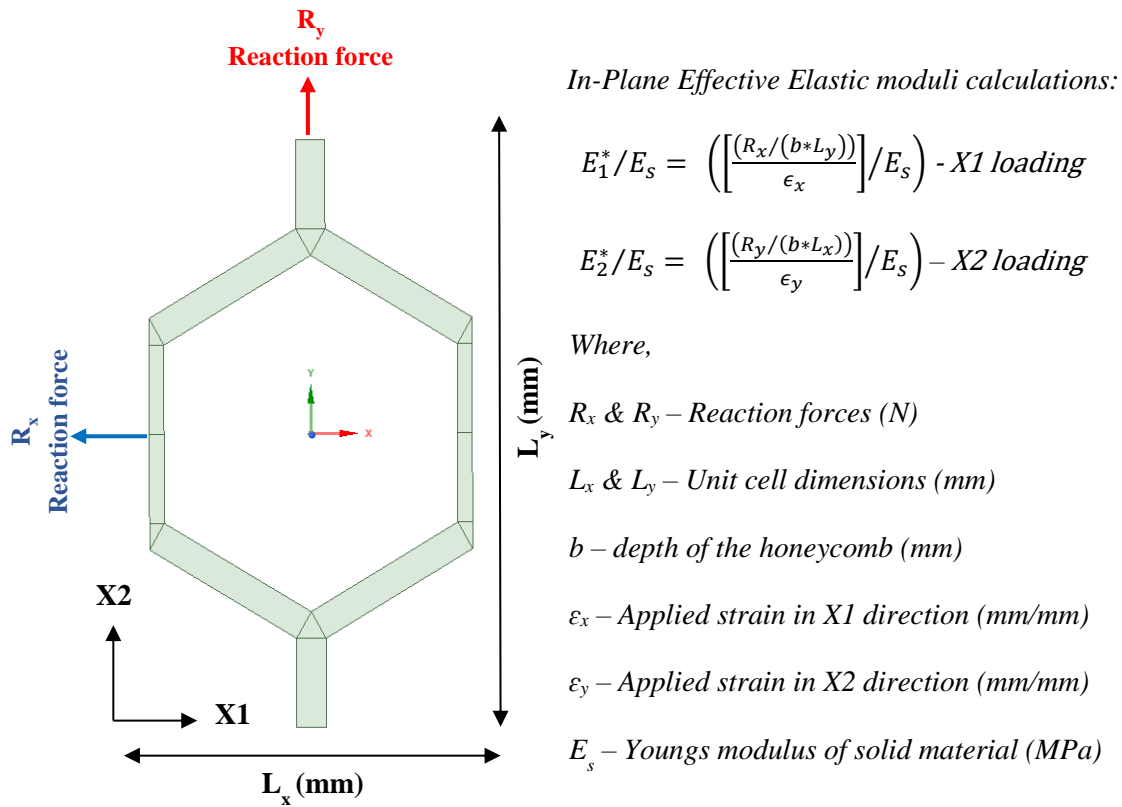


Figure 13: In-plane elastic moduli calculations

2.3 Mesh refinement study

The 2D planar model of the honeycomb unit cell is discretized into beams and triangular nodes. These constraints help to control the number of elements across the width of the beam. The full beam and half beam are constrained to have 10 and 5 elements, respectively. The numerical model uses the PLANE 183 element, which is quadratic, has eight nodes, and supports generalized plane strain conditions. In addition, this element has plasticity, hyperelasticity, stress stiffening, large deflection, and large strain capabilities. Due to the aforementioned non-linear deformation capabilities, this element type is ideal for analyzing the local mechanical response within the elastic-plastic material domain. Figure 14 illustrates the meshing constraints defined in the honeycomb unit cell.

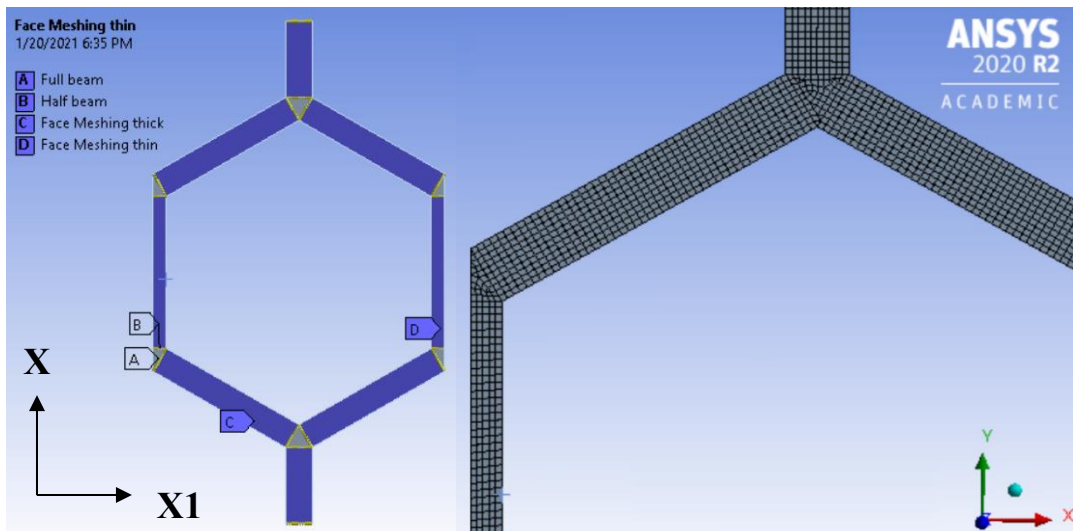
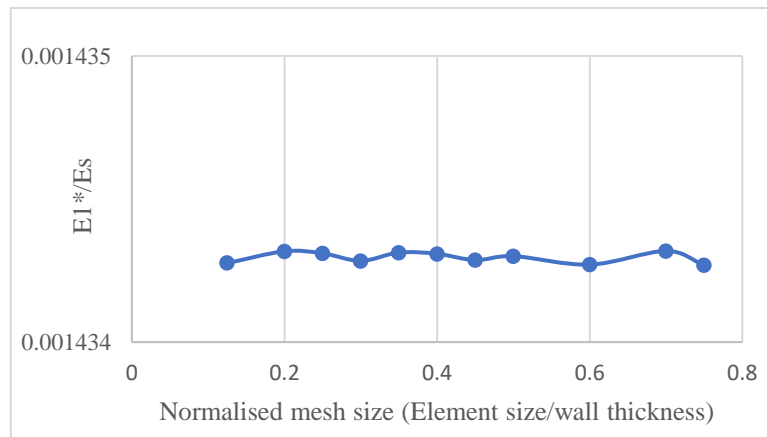
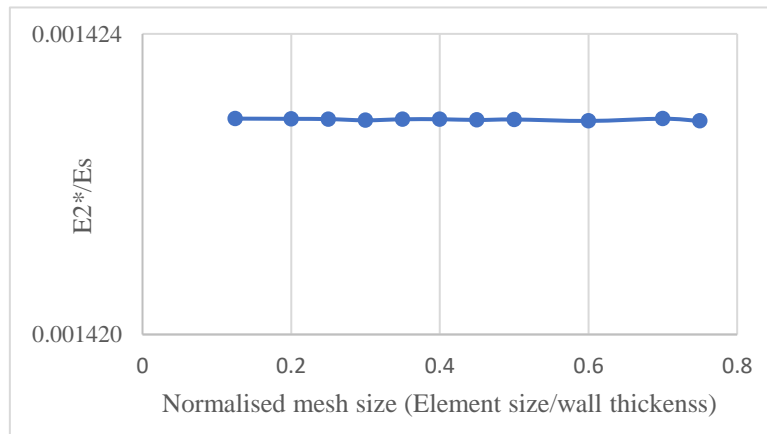


Figure 14: Numerical model - unit cell meshing constraints

The mesh convergence study for X1 and X2 compression of the honeycomb unit cell was conducted by fixing the design parameters and varying the mesh element size. The convergence of the effective in-plane elastic modulus is illustrated in Figures 15(a) & (b), respectively. The numerical model gives good convergence for in-plane elastic moduli and is considered numerically stable for further analysis and validation studies with a normalized mesh size of 0.0125.



(a)



(b)

Figure 15: In-plane elastic moduli mesh Convergence study (a) X1 (b) X2 - direction

2.4 Numerical model validation study

The accuracy of the periodic numerical model is verified by validating it against the Malek-Gibson analytical model for uniform honeycombs without plateau borders or corner radii. The numerical model was analyzed with constant cell diameter and varying wall thickness for the validation study. The respective in-plane elastic properties were calculated from the numerical model and compared with the analytical model. At higher t/l ratios (or relative densities), the numerical model started to deviate from the analytical relationship. The in-plane elastic moduli plot for X1 and X2 loading comparing the numerical and analytical is illustrated in Figure 16.

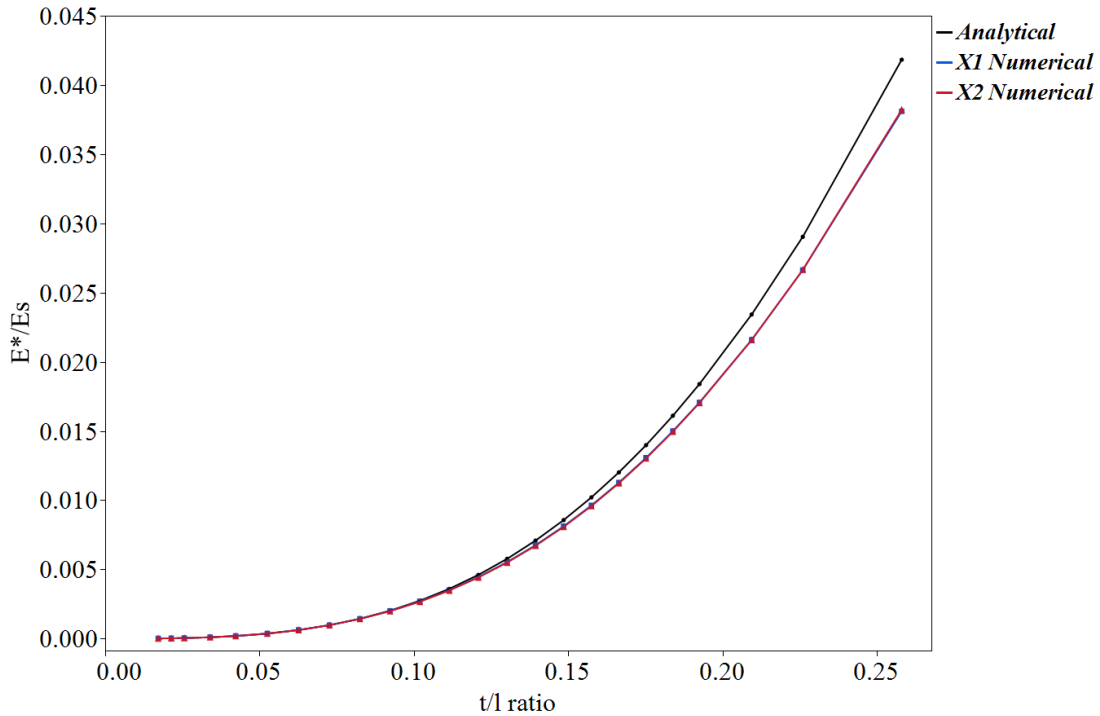


Figure 16: Comparing in-plane elastic modulus of a numerical model with Malek & Gibson analytical model

As expected, the numerical in-plane elastic modulus shows isotropy between the X1 and X2 loading conditions, supporting the appropriateness of the boundary conditions used. The deviation between the numerical and analytical models, particularly at high t/l values, is attributed to the triangular node deformation assumptions. Malek and Gibson neglect the triangular node's deformation and assume it to be rigid, as is commonly done to simplify analytical modeling. Simone et al.[17] and Warren et al. [18] also assumed the triangular nodes remain rigid. To verify if this was the cause of the discrepancy, the honeycomb unit cell elastic in-plane mechanical properties were numerically calculated with the rigid triangular node assumption and plotted against the analytical model, as seen in Figure 17, showing much better agreement.

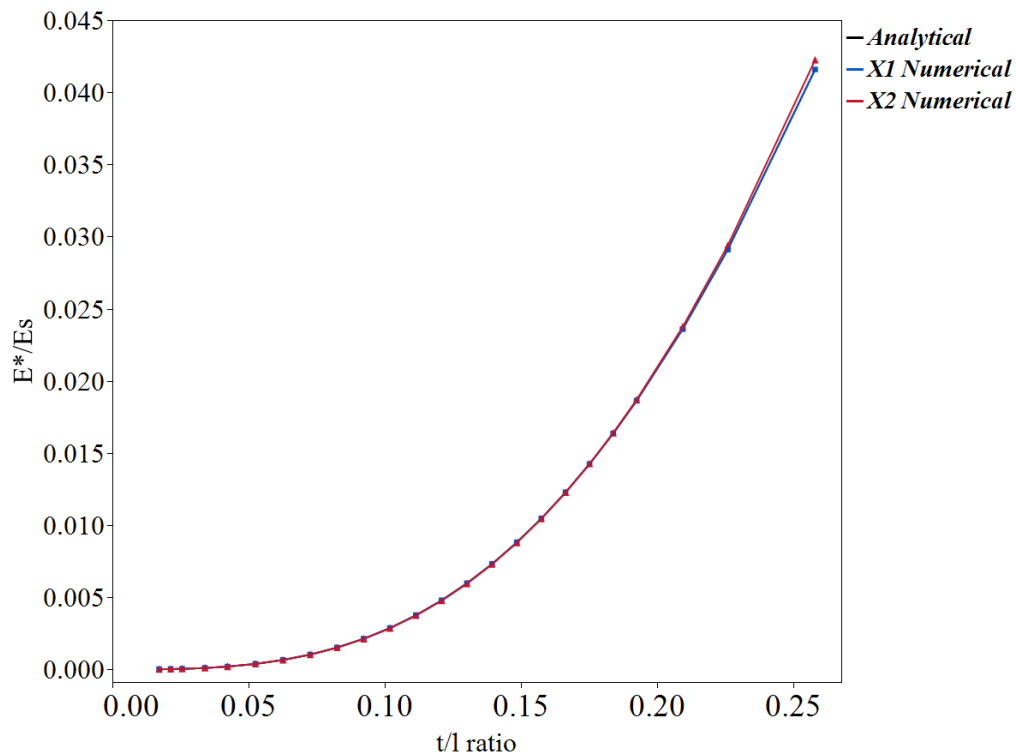
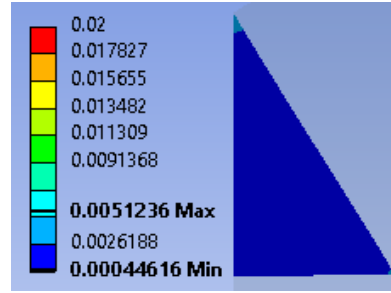
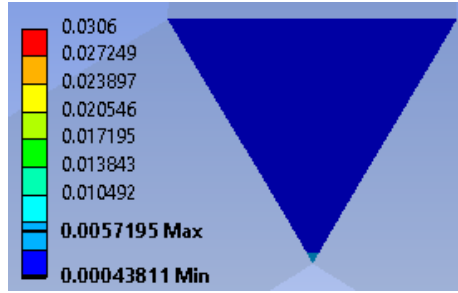
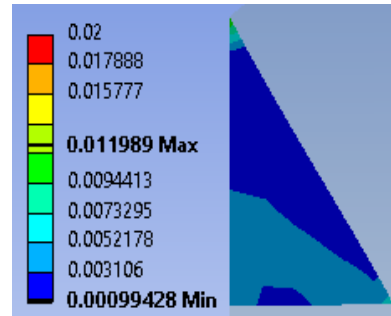
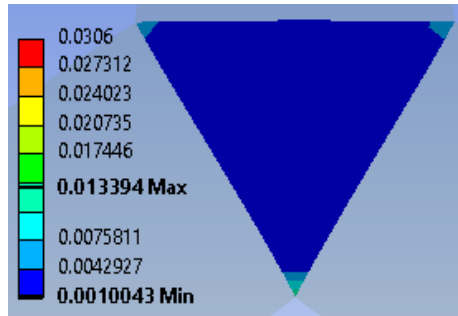


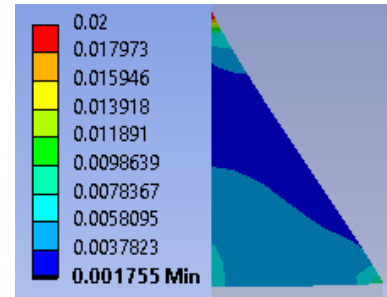
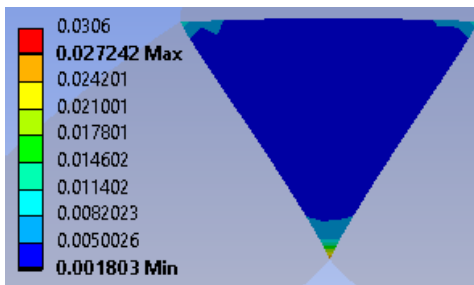
Figure 17: Updated numerical model elastic moduli properties plot with rigid triangular nodal assumption against the analytical model



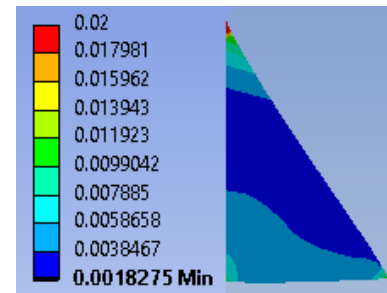
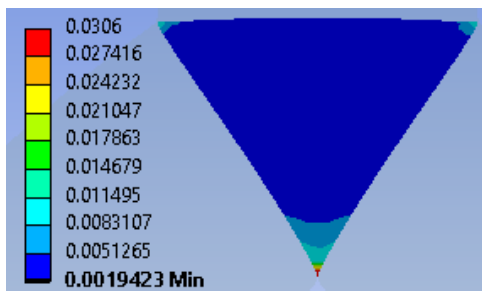
(a) t/l ratio: 0.042



(b) t/l ratio: 0.102



(c) t/l ratio: 0.226



(d) t/l ratio: 0.318

Figure 18: Nodal deformation with increment in t/l ratio

The variation in the nodal deformation is illustrated with the help of normalized equivalent elastic strain contour plots at varying t/l ratios in Figure 18 justified the deviation from the Malek and Gibson analytical model. In addition, the validation study verified the accuracy and the periodicity of the numerical analysis of honeycombs without a corner radius.

The validation of honeycombs with a corner radius or plateau borders is checked with the Chung-Huang analytical model. In this validation study, the corner radius of the honeycomb unit cell is varied parametrically, keeping the wall thickness and cell diameter constant. The results from Figure 19 suggest reasonable periodicity between the X1 and X2 in-plane compression loading. The deviation from the analytical model is attributed to the rigid triangular node assumptions and neglecting the shear deformation within the honeycomb unit cell.

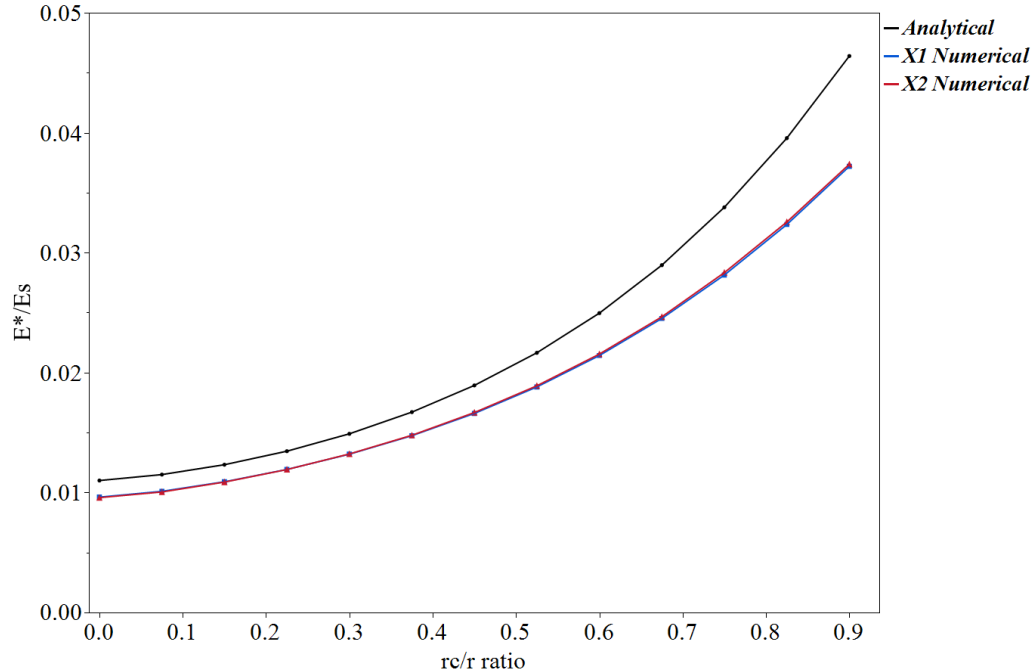


Figure 19: Numerical model vs. Chuang-Huang plateau border model

CHAPTER 3

PARAMETRIC DESIGN STUDY

Having validated the FE unit cell model, a parametric DOE (Design of Experiments) study was conducted to study the local mechanical response of a honeycomb unit cell with varying relative densities and circularities. The design parameters varied in the DOE study are presented in Table 1.

Table 1: DOE design table

Cell Diameter (mm)	Thickness levels (mm)			Corner Radius levels (mm)	
4	0.2000	0.2667	0.3333	0.2	0.2111
	0.4000	0.4667	0.5333	0.4222	0.6333
	0.6000	0.6667	0.7333	0.8444	1.0556
		0.8000		1.2667	1.4778
				1.6889	1.9000
6	0.3000	0.4000	0.5000	0.3	0.3222
	0.6000	0.7000	0.8000	0.6444	0.9667
	0.9000	1.0000	1.1000	1.2889	1.6111
		1.2000		1.9333	2.2556
				2.5778	2.9000
8	0.4000	0.5333	0.6667	0.4	0.4333
	0.8000	0.9333	1.0667	0.8667	1.3000
	1.2000	1.3333	1.4667	1.7333	2.1667
		1.6000		2.6000	3.0333
				3.4667	3.9000
10	0.5000	0.6667	0.8333	0.5	0.5444
	1.0000	1.1667	1.3333	1.0889	1.6333
	1.5000	1.6667	1.8333	2.1778	2.7222
		2.0000		3.2667	3.8111
				4.3556	4.9000

A total of 400 design points are parametrically generated and analyzed with the validated unit cell numerical model using the Nylon 12 material model (Appendix A), which is the same material used in the experimental study discussed in the next section. The benefit of conducting this parametric 2D honeycomb unit cell study is reducing the

computational effort required and simulation run time compared to simulations with full-field honeycombs. The total simulation run time for the 400 design points using a 2D planar unit cell model was around 6 hours. A full field simulation of a honeycomb panel would take approximately 60 hours with the same CPU processing power.

The key metrics considered for this DOE study are the geometric efficiency - $((E_i^*/E_s)/(\rho^*/\rho_s))$ and Normalized max corner stress - (σ^*/σ_{ys}) . Berger et al. [19] coined the term geometric efficiency to describe the effective stiffness of a cellular material independent of its composition or material density. In general, this metric is used to isolate the contribution of the cellular structure geometry towards the overall stiffness characteristics from the underlying material used in its construction for a given relative density. The normalized max corner stress is defined as the maximum equivalent Von-mises stress numerically evaluated in the vicinity of the corner radius (Figure 20) normalized by the material's yield stress. The significance of this parameter is that it characterizes the effective stress distribution with the introduction of a corner radius and can be related to the onset of plasticity.

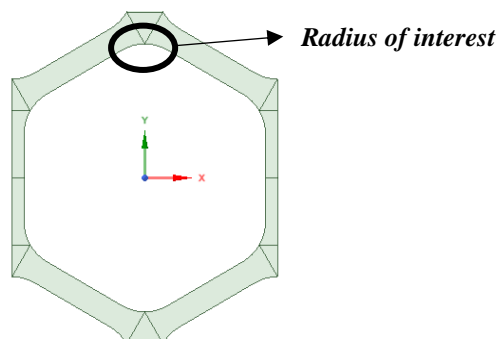


Figure 20: Corner radius stress evaluation path

Figure 21 illustrates some examples of the 2D planar unit cell design points parametrically varied using Spaceclaim and analyzed in ANSYS MECHANICAL 2020 R2. The local mechanical response of a honeycomb unit cell is studied through efficiency plots and response surface methodology plots in the following sections.

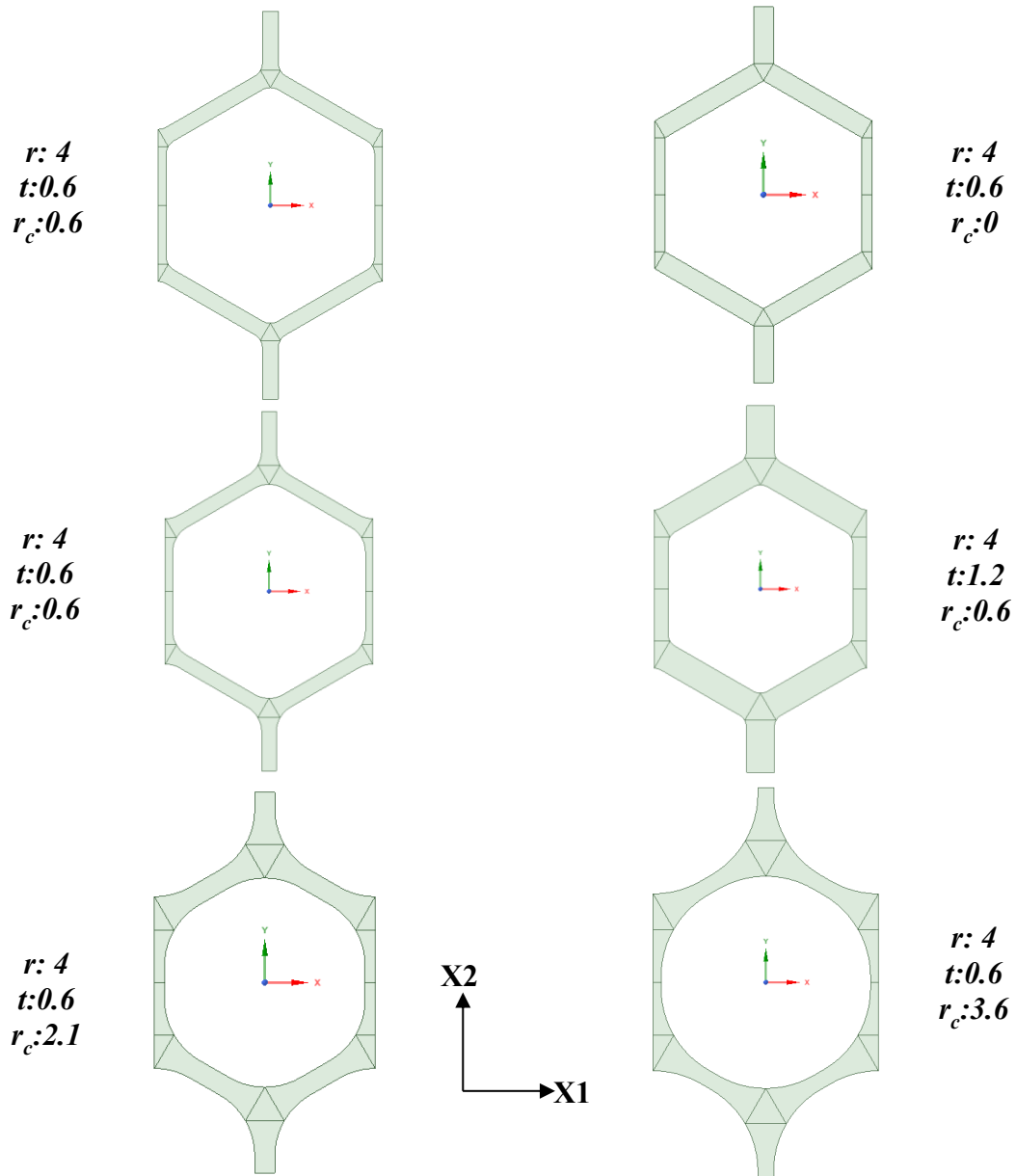


Figure 21: Honeycomb unit cells with varying geometric parameters (All units in mm)

3.1 Mechanical Response study

This DOE study explores the relationship between geometric efficiency and Normalized max corner stress and identifies the optimal geometric parameters. Figure 22 illustrates the plot comparing stress and stiffness characteristics of honeycombs with a varying cell length ratio (t/l) and circularity (r_c/r) evaluated with a constant strain of 0.001.

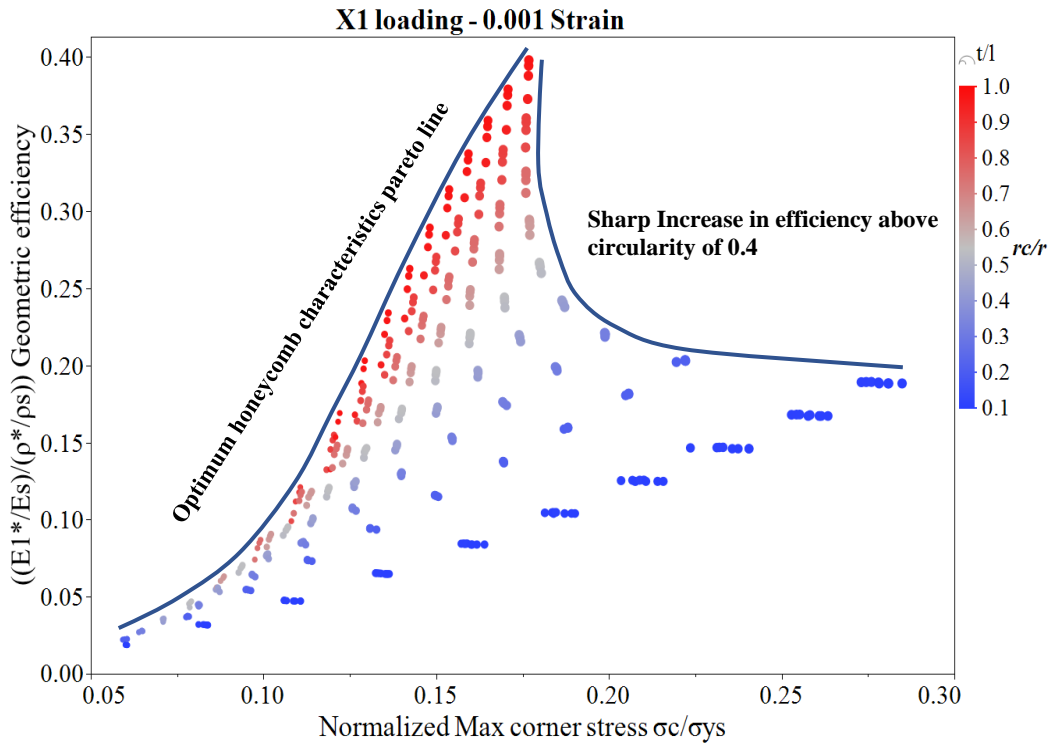


Figure 22: Geometric efficiency vs. Normalised Max corner stress _

The top-left corner in the plot represents the optimum region of the honeycomb unit cell, considering its stress and stiffness behavior. The varying color gradient from blue to red indicates increasing circularity (r_c/r), and the growing size of the data points corresponds to the increase in cell length ratio (t/l). The Pareto line at the optimum region highlights the design points with the maximum geometric efficiency and minimum stress characteristics. Additionally, it was observed that above a circularity of about 0.4, the

geometric efficiency increases sharply with a steady reduction in the normalized max corner stress. Hence, an optimal balance exists between the cell length ratio and circularity that minimizes the normalized max corner stress for a specific honeycomb unit cell geometry.

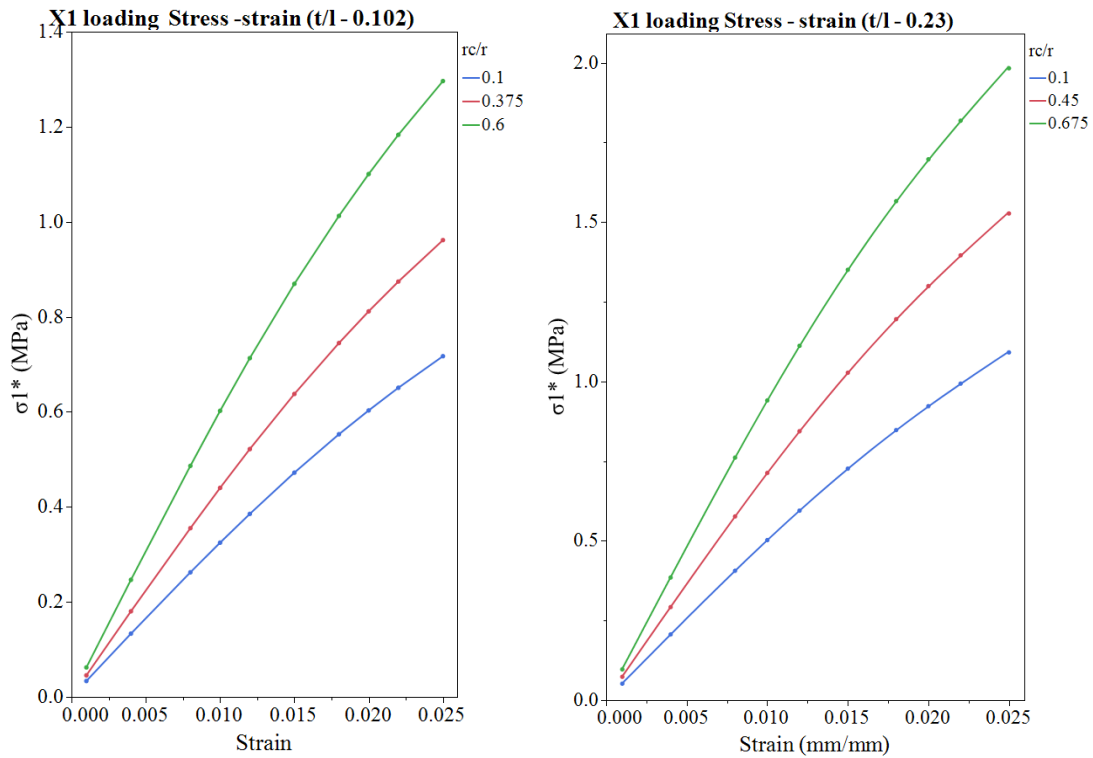


Figure 23: Onset of plasticity with varying t/l and r_c/r ratios

Before analyzing the stress and stiffness of honeycombs with varying t/l and r_c/r ratios, a plasticity study was conducted (Figure 23) where the effective stress and strain of the honeycomb unit cells were plotted against each other. In general, it was observed from the stress-strain plots that the honeycombs started to deform plastically below an effective strain of 0.01. Therefore, the region below this threshold can be characterized as the linear-elastic region, whereas the deformation at higher strains corresponds to the elastic-plastic domain. The applied strain was selected based on this plasticity study

which suggested that from a unit cell perspective, the onset of plasticity at the corner nodes starts from a strain slightly below a strain of 1%.

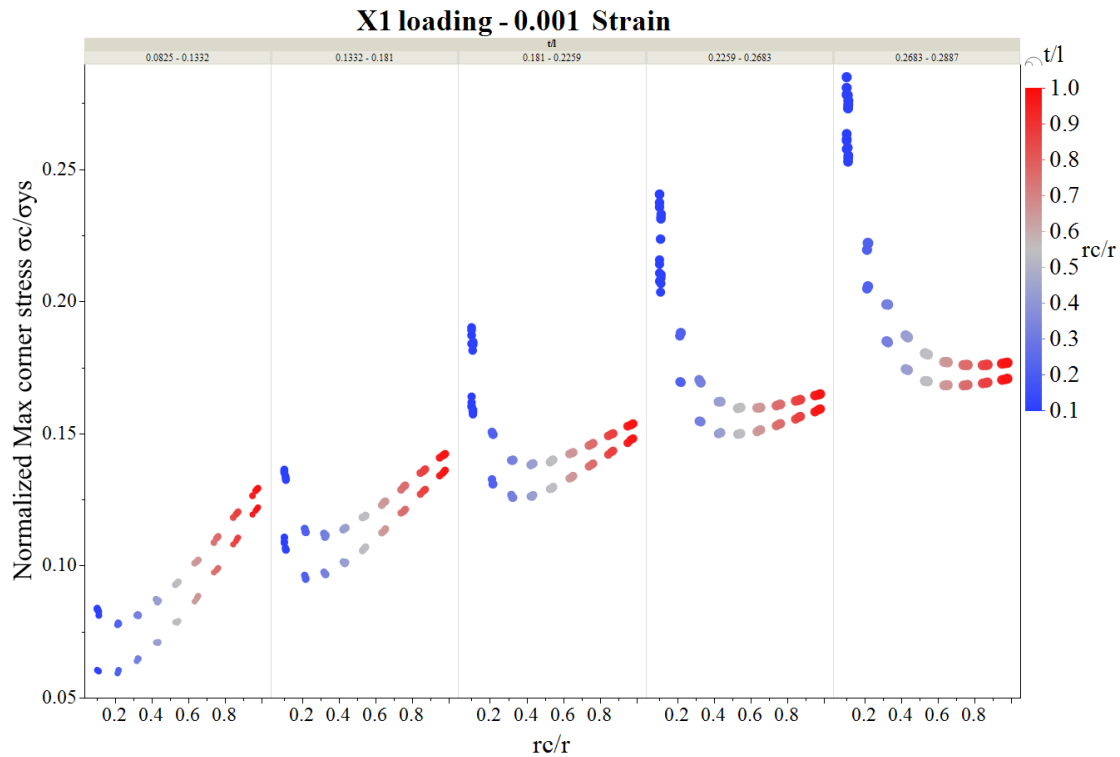


Figure 24: Variation of max corner stress with circularity (Linear-Elastic)

Figure 24 helps visualize the optimum relationship between the geometric parameters graphically within the linear elastic region (at a strain ϵ of 0.001). The results indicate that the optimal corner radii that aids with stress reduction increase with increasing t/l ratio. Additionally, in the Elastic-plastic domain (at a strain ϵ of 0.01), the variation of the plastic strain is consistent with the stress at the corners with different circularities and t/l ratios. These trends are compared with stress contours (Figure 27) of the unit cell with increasing circularity

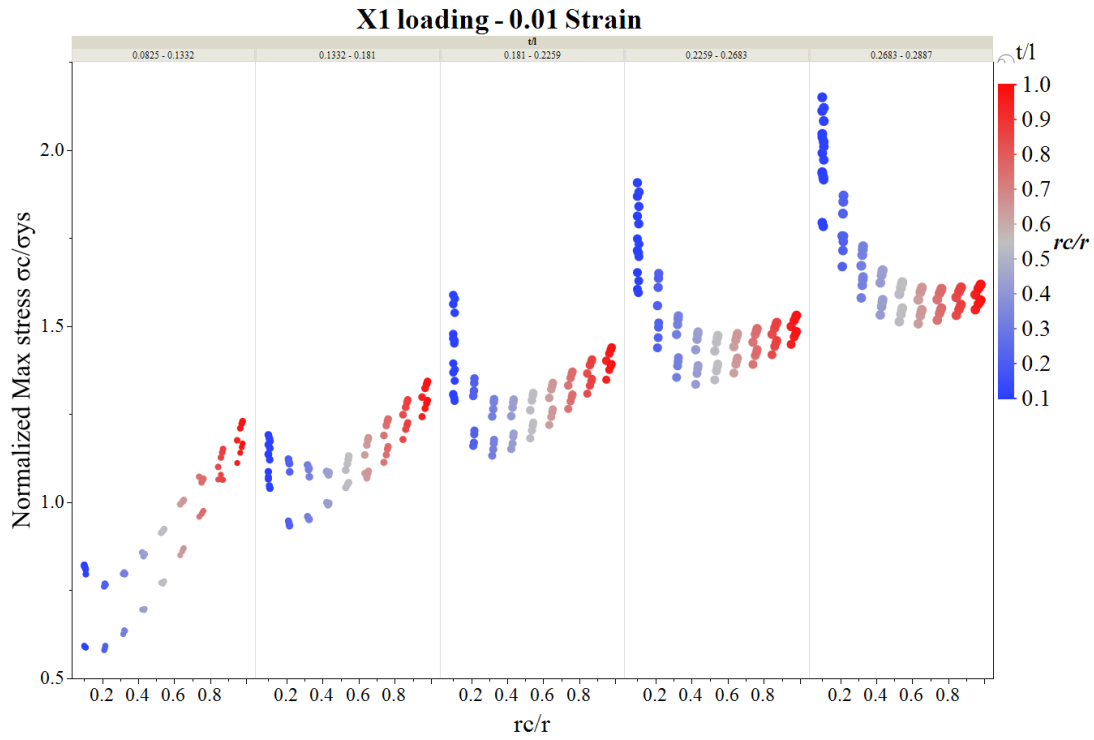


Figure 25: Variation of max corner stress with circularity (Elastic-plastic)

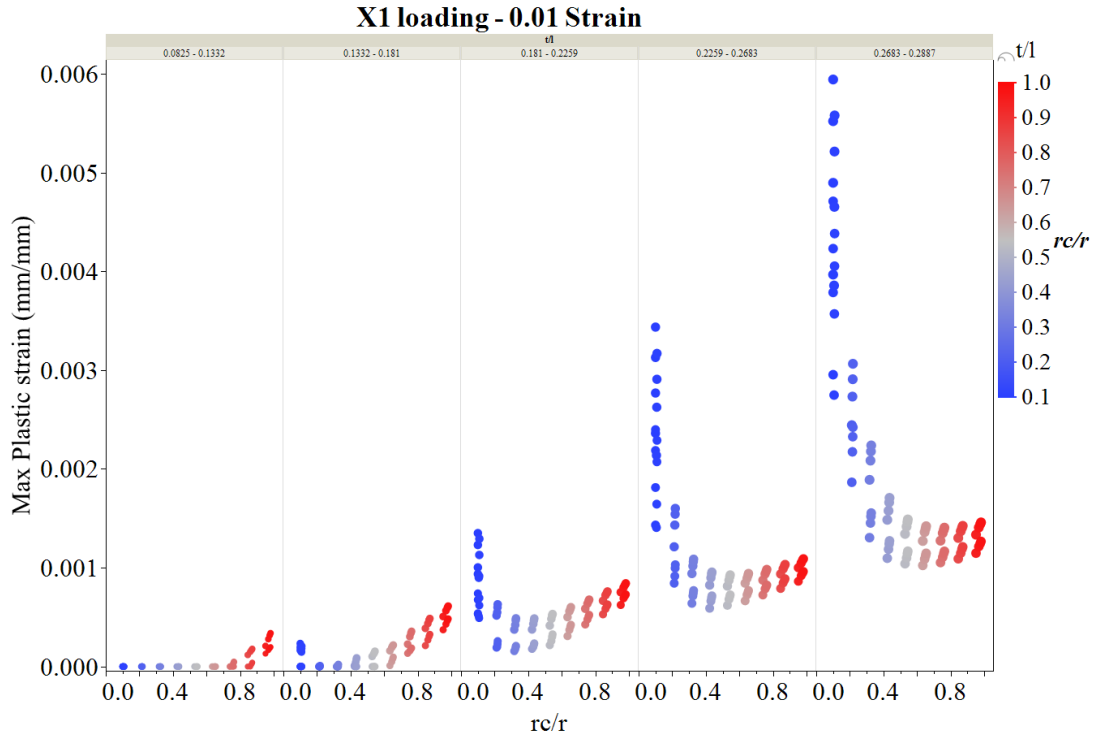


Figure 26: Variation of a max plastic strain with circularity (Elastic-plastic)

Figure 27 suggested that the corner radius delocalizes stress concentration from the middle of the corner towards the corner radius's start and endpoint, which is a plausible explanation for the stress reduction. This delocalization behavior observed at the corner radius continuum arc is consistent with Yang et al. [12], where they postulated that the plastic hinging occurred at the transition zone from constant to the variable thickness (Figure 8(a)) when the stress approached the materials yield limit.

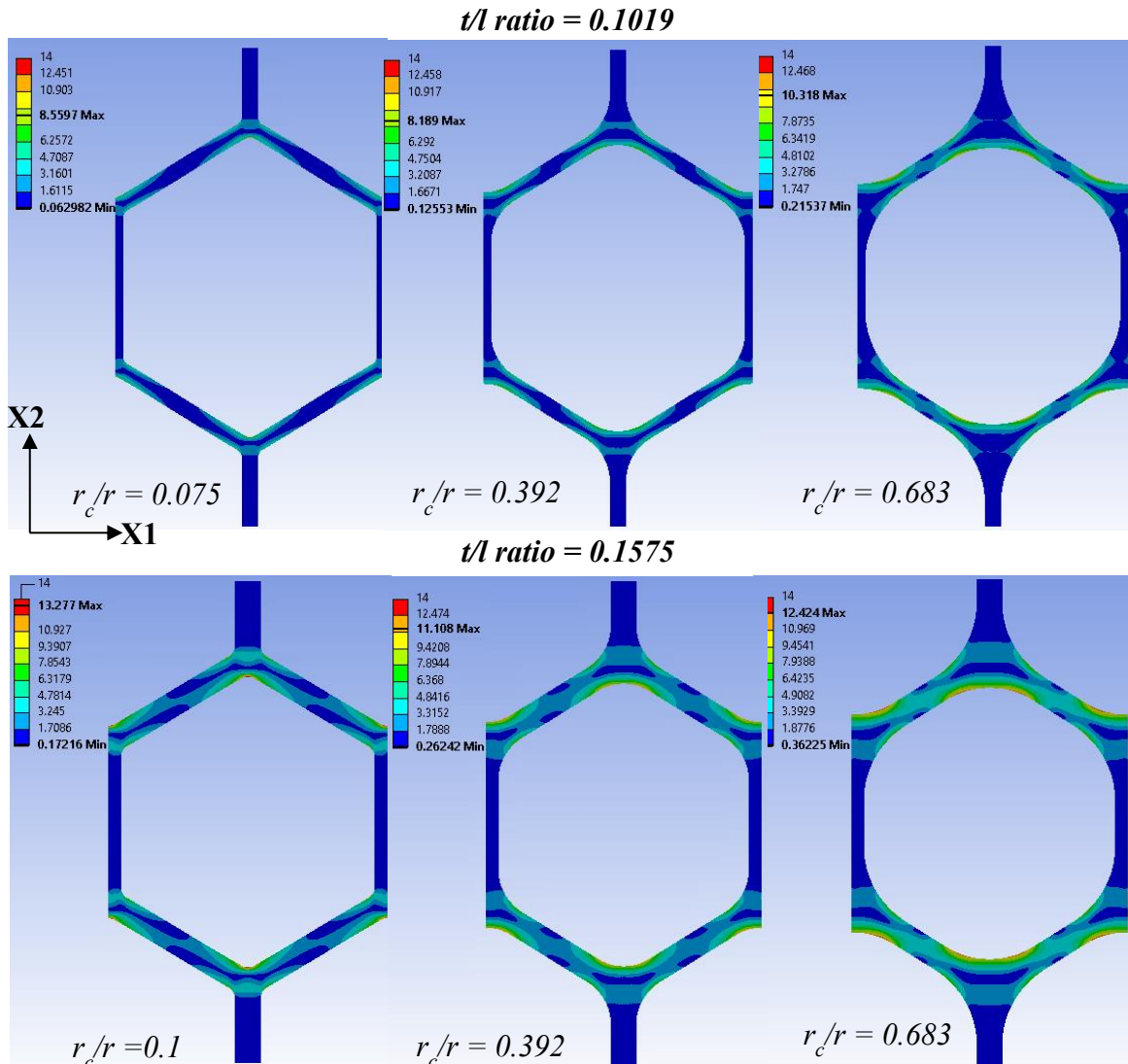


Figure 27: Evolution of stress distribution of unit cell with increasing circularity

3.2 Response Surface Methodology

Response Surface Methodology (RSM) is a set of mathematical and statistical techniques used to define a functional relationship between a response of interest (in this case, geometric efficiency and normalized max corner stress) and associated input variables (t/l - Cell length ratio and r_c/r – circularity). In general, the unknown relationship of the response to the factors is approximated by a low-degree polynomial model. The Composite Central Design (CCD) algorithm generates the data points for the factors under consideration. These design points are numerically evaluated with the unit cell model and listed in Table 2.

Table 2: RSM design table

Cell diameter (mm)	r_c/r ratio Circularity (Factor -1)	t/l ratio Cell length ratio (Factor-2)	Normalized max Corner stress (σ^*/σ_{ys}) (Response)	Geometric Efficiency $((E1^*/E_s)/(\rho^*/\rho_s))$ (Response)
4	0.10555	0.082479	0.123	0.0172
4	0.10555	0.288675	0.499	0.1755
4	0.7389	0.185577	0.271	0.1818
4	0.10555	0.185577	0.316	0.0813
4	0.7389	0.082479	0.199	0.0682
4	0.7389	0.288675	0.322	0.2922
4	0.422225	0.185577	0.249	0.1164
4	0.422225	0.082479	0.145	0.0310
4	0.422225	0.185577	0.249	0.1164
4	0.422225	0.288675	0.341	0.2218

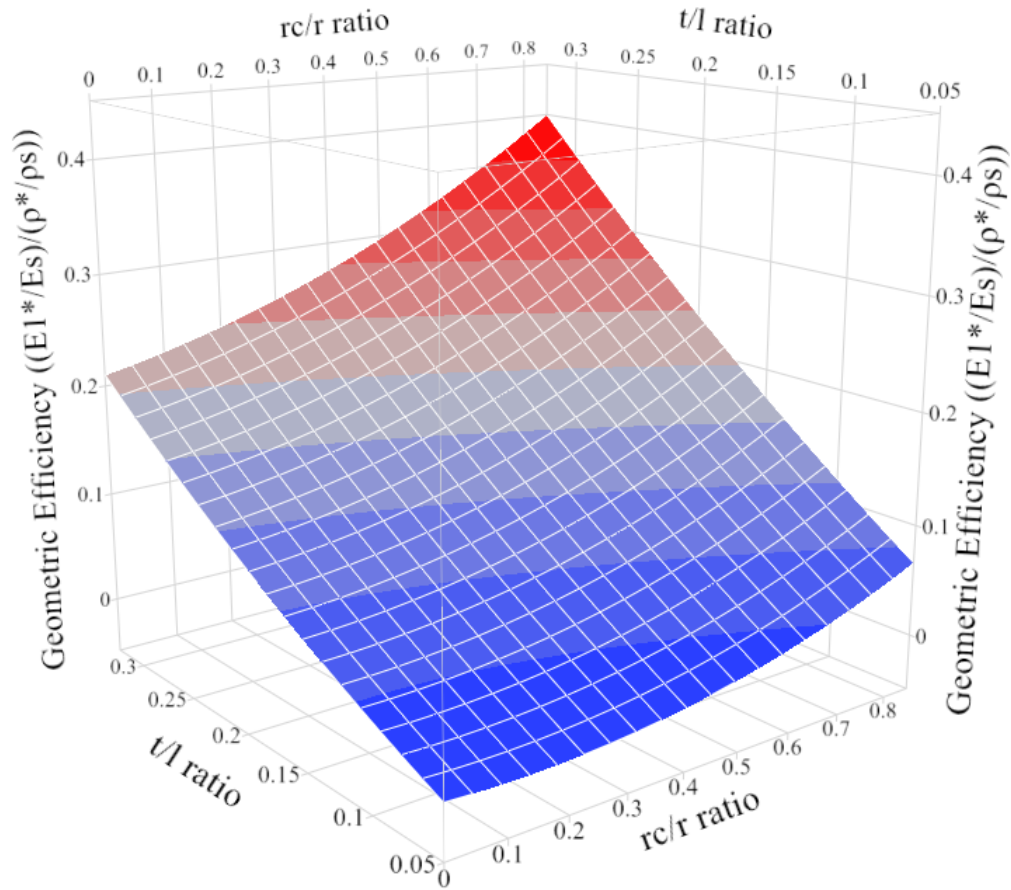


Figure 28: RSM plot of geometric efficiency varied with t/l ratio and r/r ratio

Figure 28 illustrates the response surface of geometric efficiency, which is maximized for varying cell length ratios (t/l) and circularities (r/r). The increase in t/l ratio has contributed towards improving the overall stiffness in honeycombs compared to the stiffness increase with the increment in corner radii. The enhanced bending resistance against in-plane compression for honeycombs with thick beam honeycombs is mainly due to the increase in strength modulus of the cell wall.

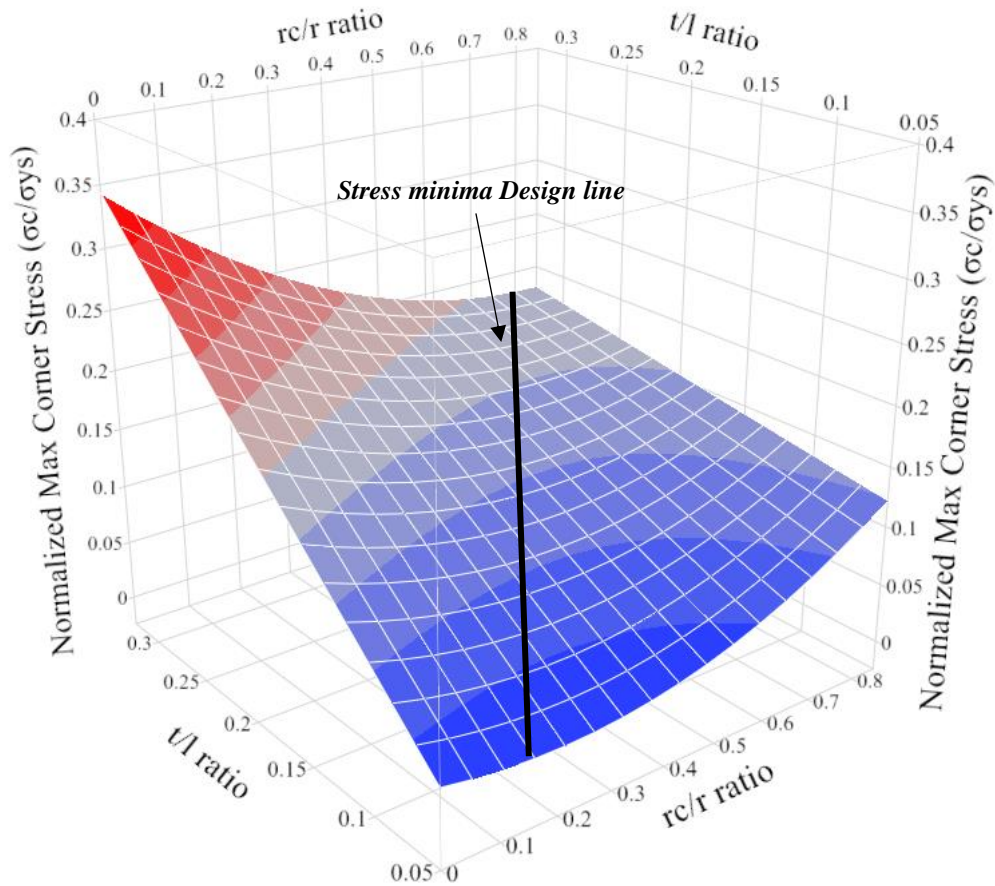


Figure 29: RSM plot of Normalized max corner stress varied with t/l ratio and r_c/r ratio

The numerically evaluated max corner stress values were set to be minimized with varying t/l and r_c/r ratios, illustrated in Figure 29. The stress minima design line highlighted in the response plot summarises the t/l and r_c/r ratio combination to give the least stress at the plateau border. Therefore, the parametric DOE study hypothesizes that circularity plays a critical structural role in minimizing the induced stresses by delocalizing the stresses away from the corner from a local mechanical standpoint and the cell length (t/l) has a significantly higher influence in improving the stiffness.

CHAPTER 4

EXPERIMENTAL STUDY

The parametric DOE study gave good insight into the local mechanical response of a honeycomb unit cell with varying relative densities and circularities. This response is compared with an in-plane compression test of 3D SLS printed honeycomb specimens in the X1 direction. This study helps to understand the global mechanical response of honeycombs with varying combinations of wall thickness and corner radius.

4.1 Honeycomb specimen design

The honeycomb specimens are parametrically designed using the SpaceClaim scripting software, as illustrated in Figure 30. All the models were designed per ISO 13314:2011 (mechanical testing of cellular solids) testing standards [20]. As per standards, the specimen width should be at least ten times the cellular solid's porosity (cell diameter). Additionally, slightly wide platens of fixed thickness were incorporated into the design that maintained good contact with the compressive supports and prevented the honeycomb cells' walls from contacting the compressor plates during the test.

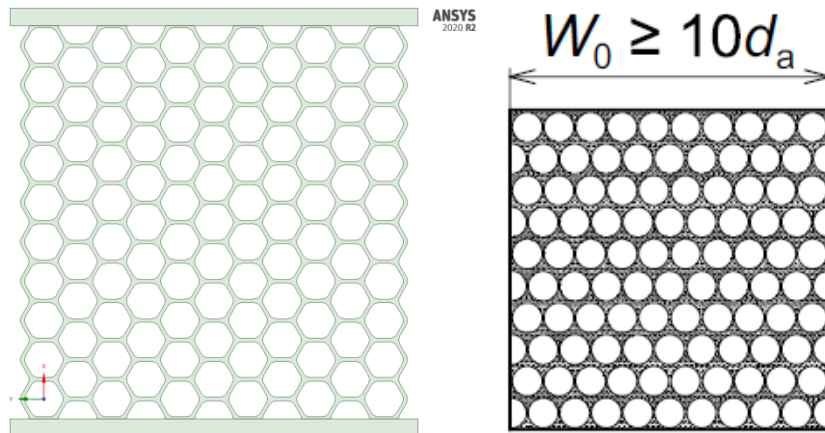


Figure 30: Honeycomb specimen design (left) and width standard (right)

Table 3 lists a total of 15 honeycomb design points developed to study the in-Plane compression behavior in the X1 direction. Specimens 1-12 were classified based on their wall thickness and had varying circularities, whereas the baseline specimens were designed without a corner radius but with varying wall thickness.

Table 3: Specimen design table

Specimen	t/l ratio (Cell length ratio)	r _c /r (Circularity)
	0.1083	
Baseline B1-B3	0.1672	0
	0.226	
		0.1083
Specimens 1-4	0.226	0.325
(High thickness)		0.542
		0.76
		0.1083
Specimens 5-8	0.1083	0.325
(Low thickness)		0.542
		0.76
		0.1083
Specimens 9-12	0.1672	0.325
(Medium thickness)		0.542
		0.76

4.2 Manufacturing and Characterization

The honeycomb specimens were 3D printed with the Formiga P110 Selective Laser Sintering (SLS) 3D printer [21] (Figure 31) using Nylon 12 Powder. Before the print is started, the raw material powder is preheated below its melting point, making it easier for the laser to sinter or increase the temperature at specific regions of the powder bed. In this additive manufacturing method, the powder is deposited in a thin layer on top of a platform within the build chamber, after which the laser scans a cross-section of the 3D model, heating the powder just below or above its melting temperature. The platform lowers by 50 – 200 microns, and the process is repeated for each layer until the parts are printed entirely. Finally, the scanned areas of the laser beam part are fused to form the 3D model. The unsintered powder supports the part during printing, eliminating the need for dedicated support structures.

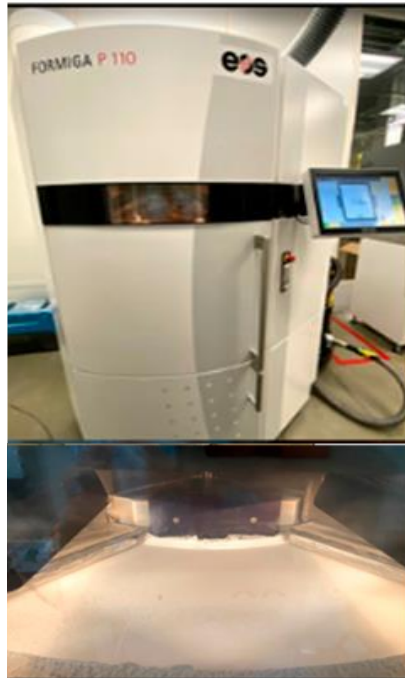


Figure 31: SLS 3D printing

The honeycomb specimens were printed in two different batches. The print orientation is specified by arranging the STL CAD files in the build chamber using the included software from the machine vendor shown in Figure 32. After the print is completed, the build chamber cools down inside the print enclosure and outside the printer to avoid warping in parts and ensure optimal mechanical properties.

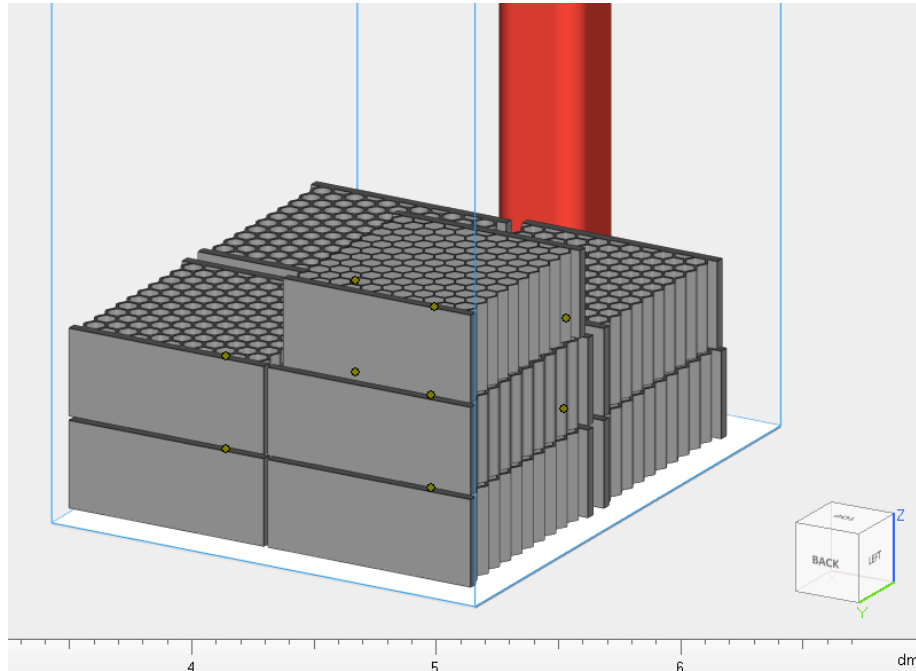


Figure 32: Honeycomb specimens arranged in the build chamber

The printed parts are removed from the build chamber and are post-processed at a separate work station to remove the un-sintered trapped powder from the honeycombs with a set of brushes and tweezers (Figure 33). The parts are then blasted (Figure 34) with glass beads to eliminate layer lines and remove unwanted protrusions such as blobs from the model's surface. The bead-blasted specimens are then washed with water and air-blasted to remove any residual particles sticking to the specimen. Finally, the

dimensions of the printed specimens were characterized using optical and physical measurements.



Figure 33: Post-processing of honeycomb specimens

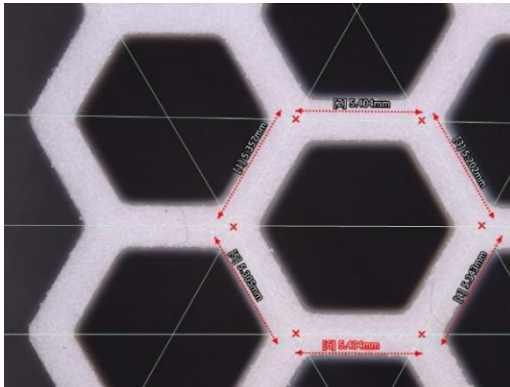


Figure 34: Bead blasting of the specimen with glass powder

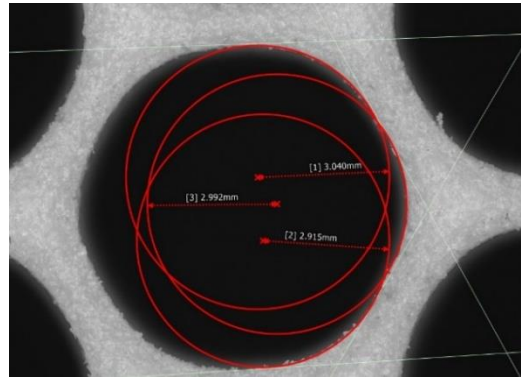
The honeycomb specimens were measured and characterized using the Keyence VR 3200 optical imaging machine (Figure 35) and a set of vernier calipers. The Keyence optical imager uses a combination of high and low magnification lenses to capture the nuanced geometric features such as the corner radius and cell length of the honeycomb specimens. In addition, the wall thickness, cell diameter, and the outer dimensions of the samples were measured with the vernier calipers. Finally, the optical and physical measurements were taken at various points and averaged to calculate the cell aspect ratio (t/l) and circularities (r_c/r) variability charts (Figure 36(e)). In general, it was observed that the measured values deviated from the design. The difference in laser beam offset value (calibration parameter in the SLS 3D printing) was identified as the root cause of this deviation, after which an entire recalibration was performed on the SLS system.



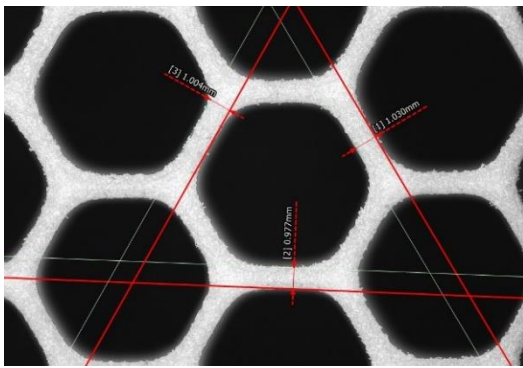
Figure 35: Keyence VR-3200 imager



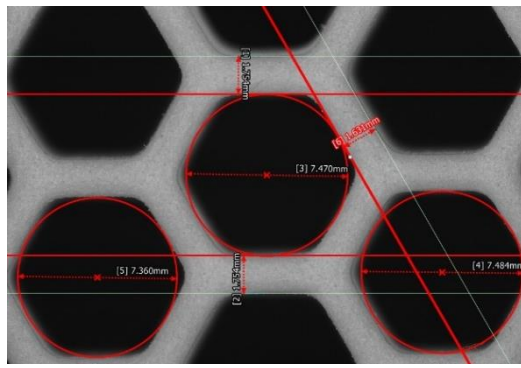
(a) Cell length measurement 12x Mag.



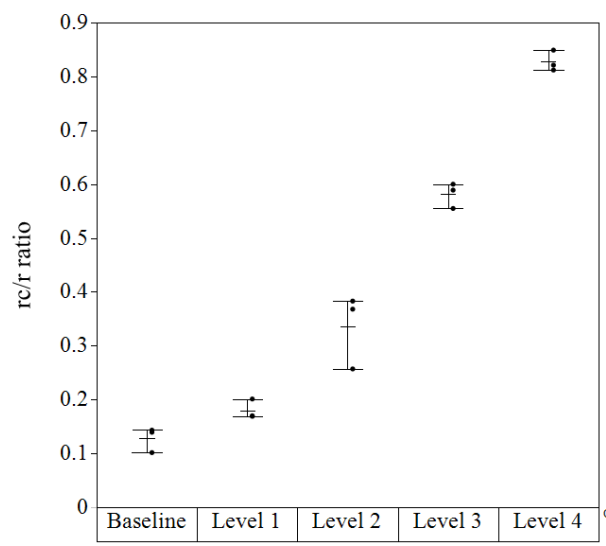
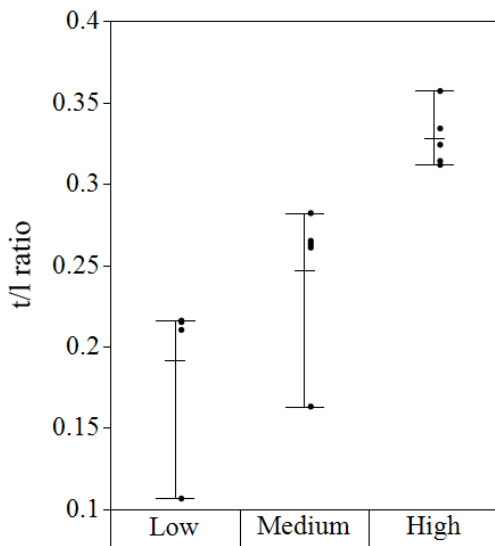
(b) Corner radius measurement 25x Mag.



(c) Wall thickness measurement 12x Mag.



(d) Cell diameter measurement 12x Mag



(e) Variability chart –increasing levels of t/l (left) & r/r ratio (right)

Figure 36: Optical measurements using Keyence imager

Table 4: Comparison between Measured and Actual t/l and r_c/r ratios

Specimen	t/l ratio		r_c/r	
	(Cell length ratio)		(Circularity)	
	Measured	Actual	Measured	Actual
Baseline	0.1087	0.1083	0.1016	0
	0.2608	0.1672	0.1432	
	0.3112	0.226	0.1393	
Specimens 1-4	0.314	0.226	0.1694	0.1083
High thickness	0.3236		0.3685	0.325
	0.3569		0.599	0.542
	0.3339		0.8486	0.76
Specimens 5-8	0.2104	0.1083	0.1699	0.1083
Low thickness	0.2151		0.3831	0.325
	0.2103		0.5887	0.542
	0.2159		0.812	0.76
Specimens 9-12	0.265	0.1672	0.222	0.1083
Medium thickness	0.263		0.35	0.325
	0.1632		0.555	0.542
	0.282		0.8211	0.76

Table 4 indicates a variation between the measured and actual design values of the honeycomb, but the specimens can still be classified based on their comparable circularity and relative density values for the compression test and also for further comparisons with the parametric DOE.

4.3 Compression test methodology

The Instron 5985 Universal Testing machine (Figure 37) with the compression testing package with the compressor plates attached to the crossheads is employed to conduct the honeycomb's in-plane compression test. The compression test method is defined using the Bluehill Universal software interfaced with the machine through which the crosshead speed and the displacement limit are set. The applied compression strain rate is 10^{-3} s^{-1} per ISO 13315:2011 cellular solids mechanical testing standards [20]. Moreover, the compression test is stopped for safety reasons when the strain reaches 70% to avoid direct contact between the compressor and exceed load capacity.

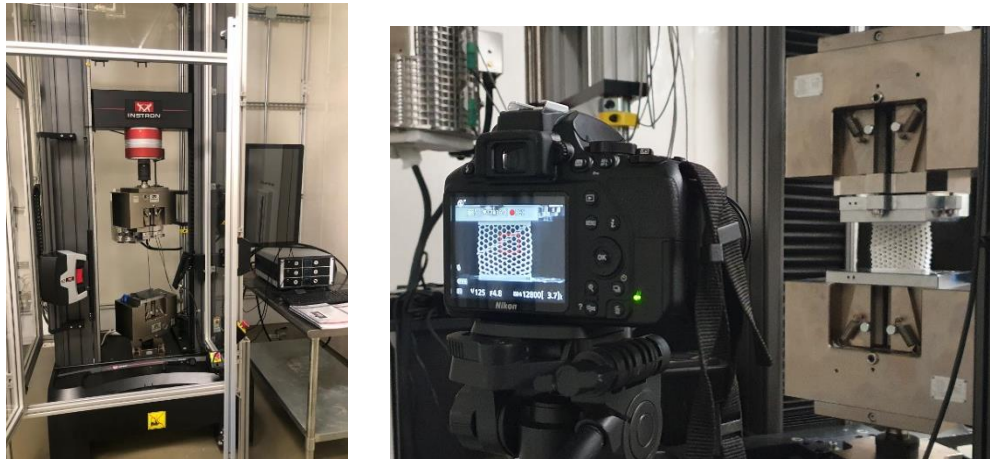


Figure 37: Instron 5985 Universal testing machine (left) and test setup (right)

Before the test starts, the honeycomb specimen is placed on the center of the bottom compressor plate. Next, it is adjusted to capture the deformation behavior with a DSLR camera. Finally, the force-displacement output data is imported into MATLAB to retrieve the stress-strain plots of the honeycomb specimens. Photographic stills of the deformation behavior at different strains for specimens 1 & 4 are illustrated in Figure 38, respectively.

4.4 Compression test results

The stress-strain curves (Figure 38) for the honeycomb specimens with a high wall thickness and varying circularity indicate that the peak stress increases with the rise in corner radius. Additionally, the thick-walled specimens at higher circularities observed the smoothness or reduction in stress peaks. Therefore, this relatively smooth stress-strain plateau (specimen 4) is analyzed and compared with a low corner radius and similar thick honeycomb (specimen 1) in Figure 39. At $\epsilon = 0.1$, specimen 1 starts to hinge plastically at the corner node interface, leading to a series of breaks and fractures. In contrast, the cell wall beams of Specimen 4 continue to yield plastically with comparatively minimum fractures. This extended plastic yielding gives credible evidence that the presence of a corner radius for a specific t/l ratio will help to smoothen the stress-strain curve for honeycomb structures.

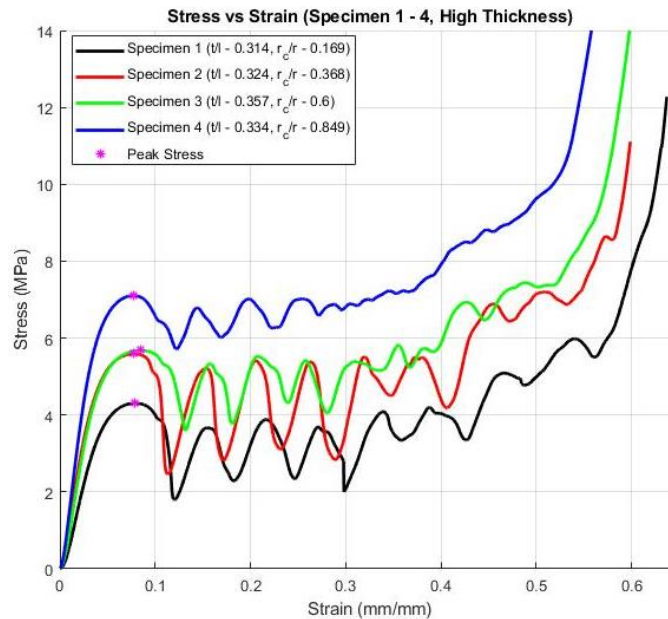
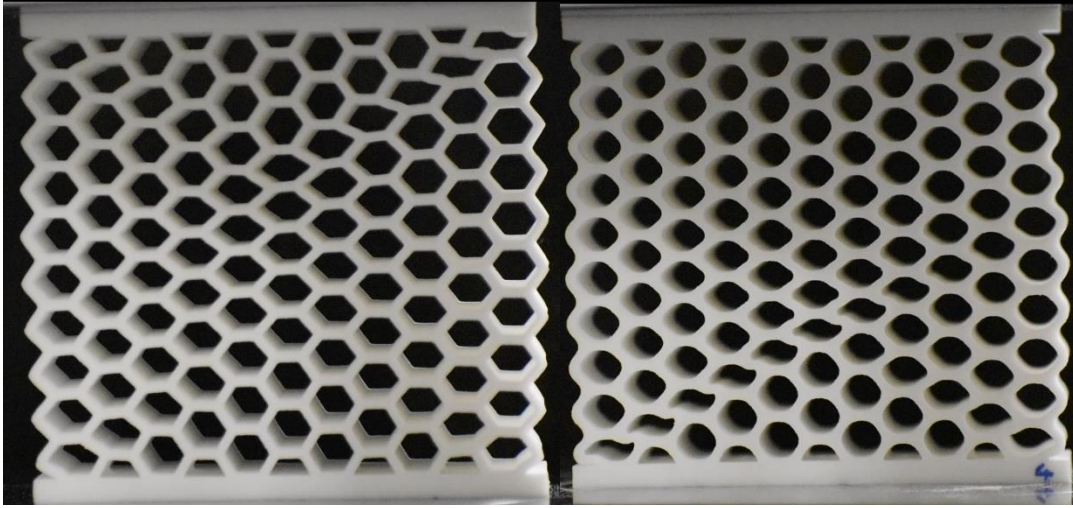


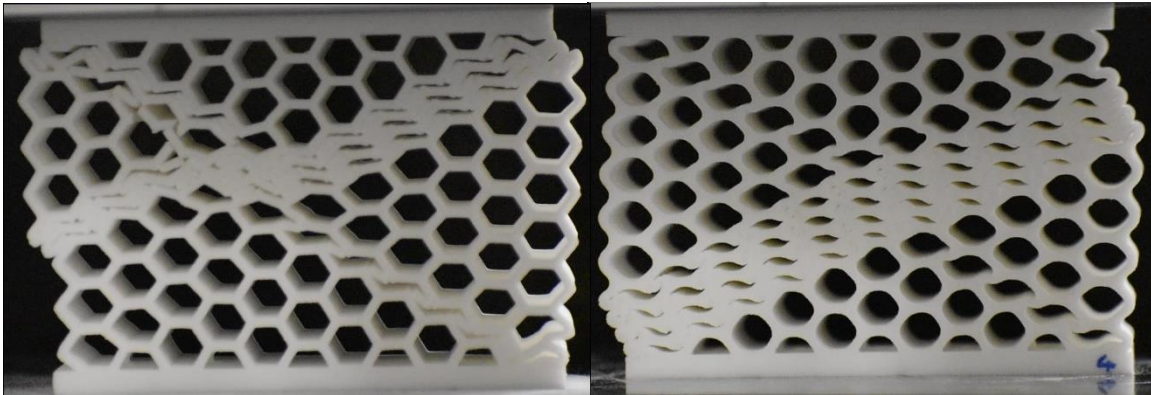
Figure 38: Compression testing results for honeycombs with high wall thickness

Specimen 1 ($t/l = 0.314$ $r_c/r = 0.169$)

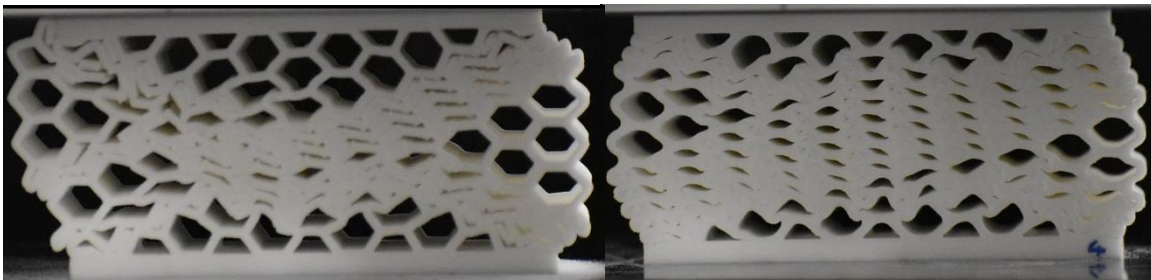
Specimen 4 ($t/l = 0.334$ $r_c/r = 0.85$)



(a) $\varepsilon = 0.1$



(b) $\varepsilon = 0.3$



(c) $\varepsilon = 0.5$

Figure 39: Comparing the deformation behavior between Specimen 1&4 at different strain intervals

The stress-strain plot (Figure 40) of the baseline specimens with fixed circularity and varying wall thickness shows that the wall thickness significantly influences the stiffness than the corner radius's contribution. To quantify this, the increase in stiffness from Baseline 1 to Baseline 3 was about 96%, whereas the stiffness rise in specimens (Specimen 1 and 4) with similar wall thickness and varying circularities was about 40%. In addition to this, the thin-walled baseline specimen (Baseline 1) had a very smooth plateau compared to the thick-walled honeycomb (Baseline 3). In Figure 41(a), for a strain of 0.1, the thick-walled specimen fails through the staircase mechanism where the cells collapse and form a step-like pattern. In contrast, the thin-walled specimen extensively deformed through elastic buckling of cell walls with relatively minimum fractures compared to the thick-walled honeycomb (Baseline 3).

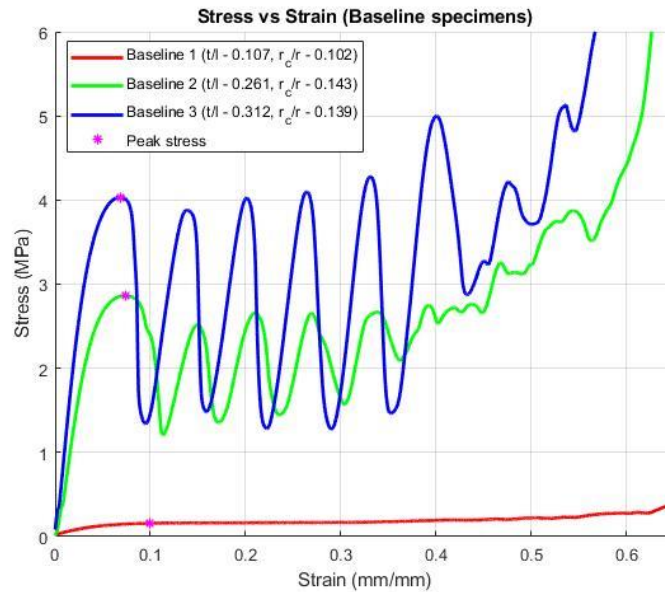
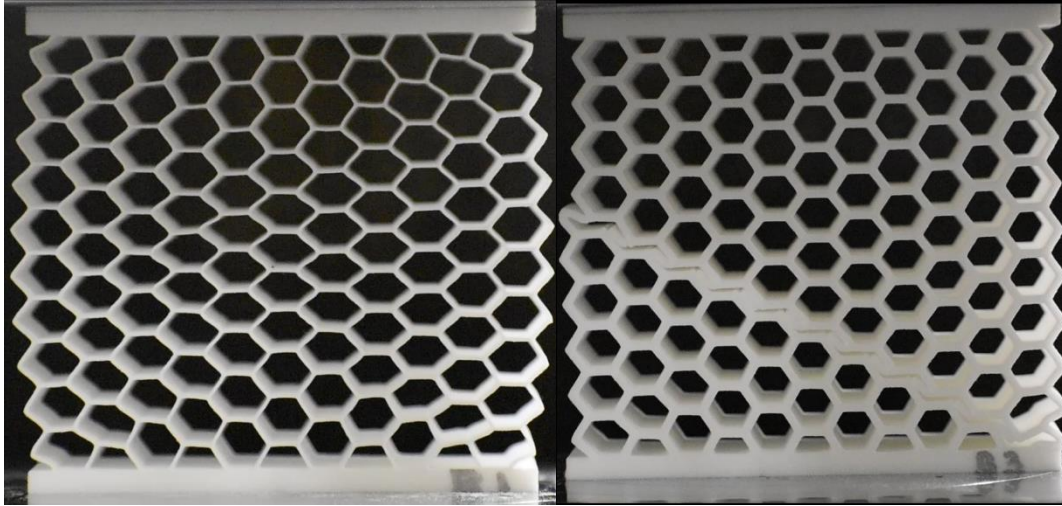


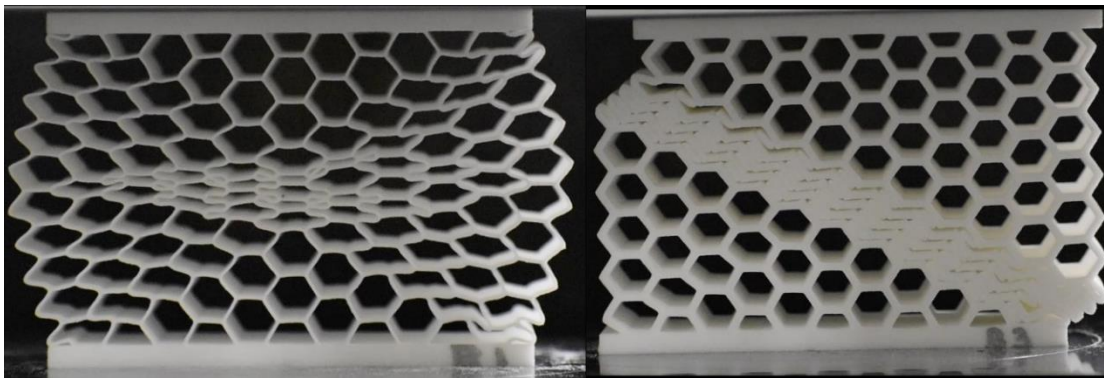
Figure 40: Compression testing results for honeycombs with baseline specimens (Fixed circularity with varying wall thickness)

Baseline 1 ($t/l = 0.107$ $r_c/r = 0.102$)

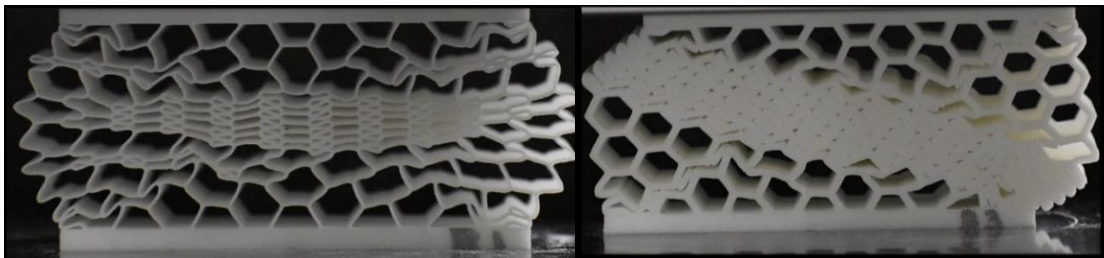
Baseline 3 ($t/l = 0.312$ $r_c/r = 0.139$)



(a) $\varepsilon = 0.1$



(b) $\varepsilon = 0.3$



(c) $\varepsilon = 0.5$

Figure 41: Comparing the deformation behavior between Baseline 1&3 at different strain intervals

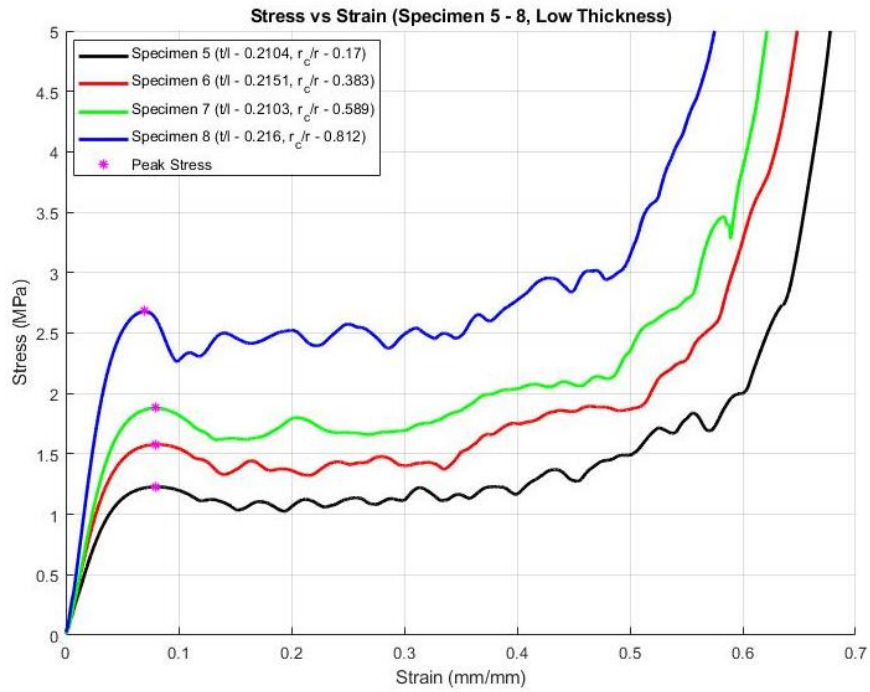


Figure 42: Compression testing results for honeycombs with low wall thickness

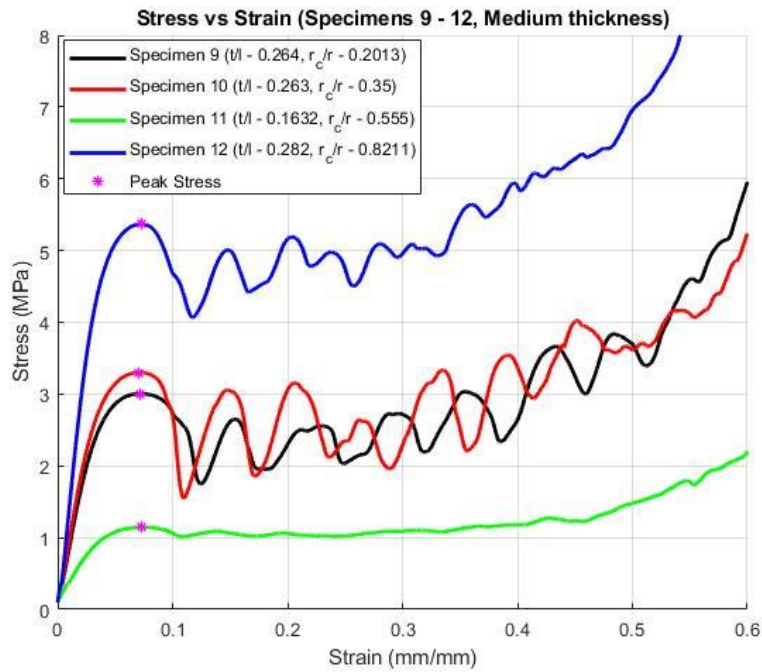


Figure 43: Compression testing results for honeycombs with medium wall thickness

The stress-strain plots of specimens with low (Figure 42) and medium wall thickness (Figure 43) showcase the deformation behavior varies for different t/l and r_c/r ratios. In general, the presence of a smooth plateau indicates that the honeycomb deforms extensively through plastic yielding or elastic buckling. In contrast, the peaks and valleys correspond to the failure of cell wall beams as the stresses exceed the yield limit and approach the point of rupture. Interestingly, the thin-walled honeycomb with low circularity (Baseline 1) and thick-walled honeycomb with high circularity (Specimen 4) had a similar smooth stress-strain plateau with extensive elastic buckling and plastic yielding (Figure 44), respectively. Therefore, the experimental study suggests that an optimum combination of cell length ratio and circularity exists to minimize the collapse of the honeycomb cells under in-plane compression and the deformation pattern transitions between smooth plateau with elastic buckling or plastic yielding varying stress peaks with cell collapse and fractures.

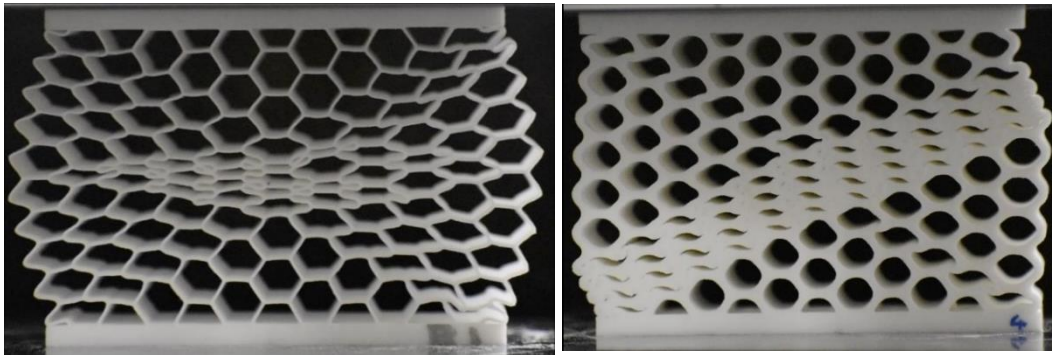


Figure 44: Elastic Buckling (left) and Plastic yielding deformation (Right)

CHAPTER 5

ANALYSIS AND DISCUSSION

The experimental and numerical study independently showed a combination of t/l ratio and r_c/r ratio that optimizes the stress and stiffness characteristics of the honeycomb structure exists. This chapter aims to characterize this behavior and explain this deformation mechanism by comparing the insights gained from the finite element unit cell study and in-plane compression tests of SLS 3D printed honeycomb specimens.

5.1 Comparing experimental trends with numerical model

The Parametric finite element DOE study for a honeycomb unit cell concluded that the degree of stress reduction at the corner nodes depends on the combination of cell aspect ratio (t/l) and circularity (r_c/r). Additionally, the delocalization of stress at the corner in the presence of a radius was identified to effectively distribute the stress over the arc of the corner radius. The experimental in-plane compression tests of SLS 3D printed honeycombs concluded that the presence of a corner radius for a specific cell wall thickness helped to smoothen the stress-strain plateau. In addition, the difference in deformation behavior was visually explained using photographic stills at different strains of the specimens under compression. The smooth plateaus corresponded to extensive cell wall bending through elastic buckling and plastic yielding. The stress-strain plots with peaks and valleys corresponded to the honeycomb cells collapsing under compression. Therefore, it is interesting to analyze how the local delocalization behavior at the corner node compares with the global yielding mechanism.

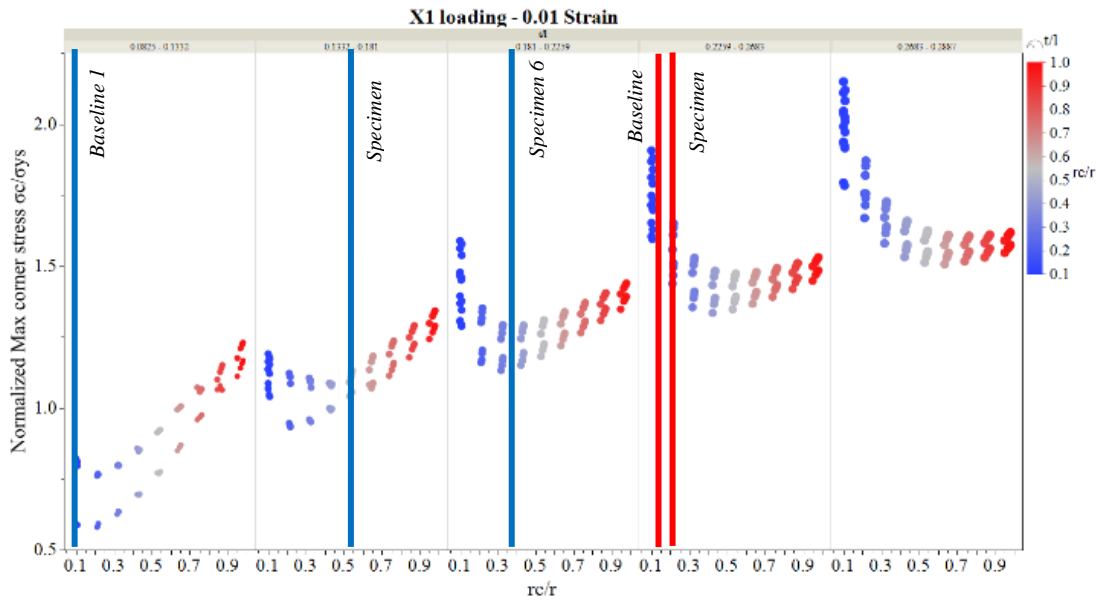
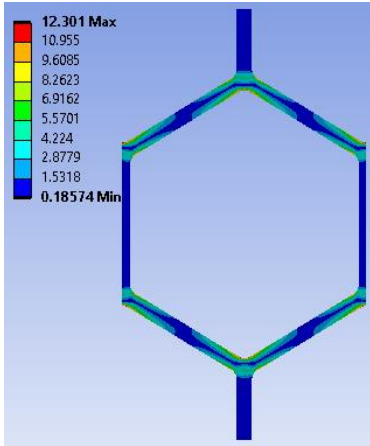
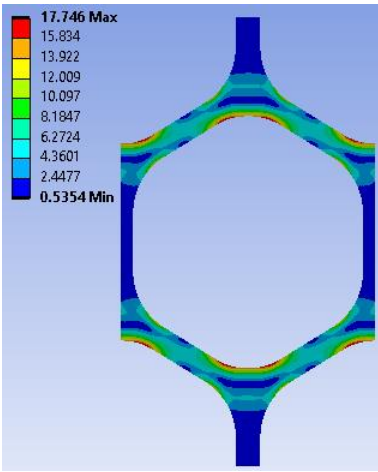
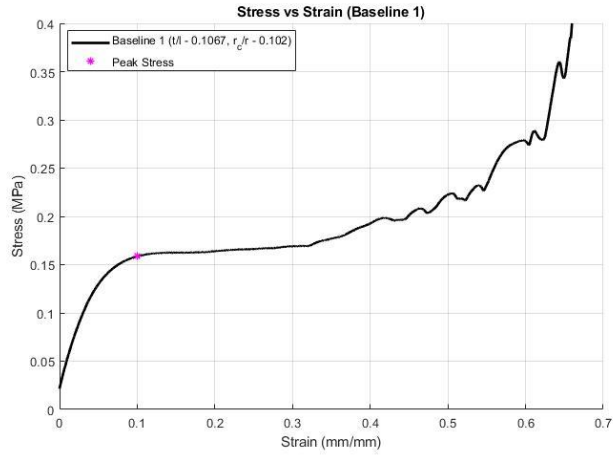


Figure 45: Comparing experimental and numerical trends

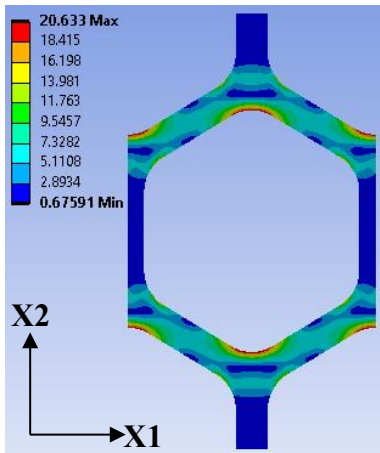
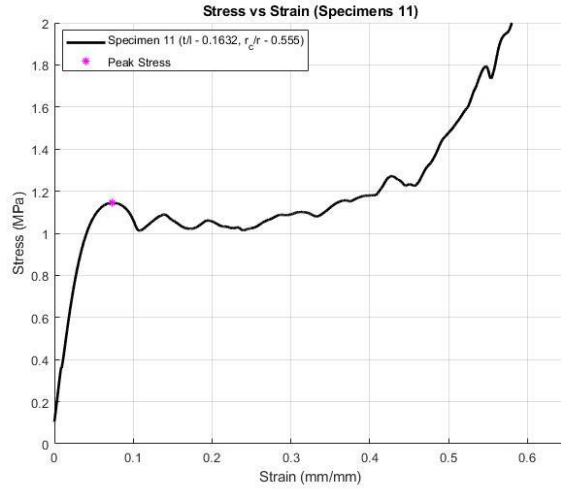
The experimental stress-strain plots were compared with the numerically evaluated normalized max corner stress graph (Figure 45). The blue lines on the chart highlight the specimens (Baseline 1, Specimen 6 & 11) with a relatively flat plateau closer to the numerical design points with low stresses at the corner. The red lines compared the specimens (Baseline 2 and Specimen 9) with high-stress peaks and cell wall failures and existed near the numerical design points with higher stress at the corner. The flat plateau behavior in Baseline 1 (low t/l and r_c/r , Figure 46(a)) was compared with the stress contours ($\epsilon=0.01$) indicates that the beams deformed through cell wall bending with minimum stresses induced at the corner node. Similarly, in specimens 11 and 6, the delocalization of stress (Figure 46(b)&(c)) at the corner radius node prevented the cell beams from fracturing prematurely and deformed primarily through bending to provide a smooth stress-strain plateau beyond its peak stress.



(a) $t/l = 0.11$ $r_c/r = 0.102$ $\varepsilon = 0.01$



(b) $t/l = 0.16$ $r_c/r = 0.56$ $\varepsilon = 0.01$



(c) $t/l = 0.215$ $r_c/r = 0.38$ $\varepsilon = 0.01$

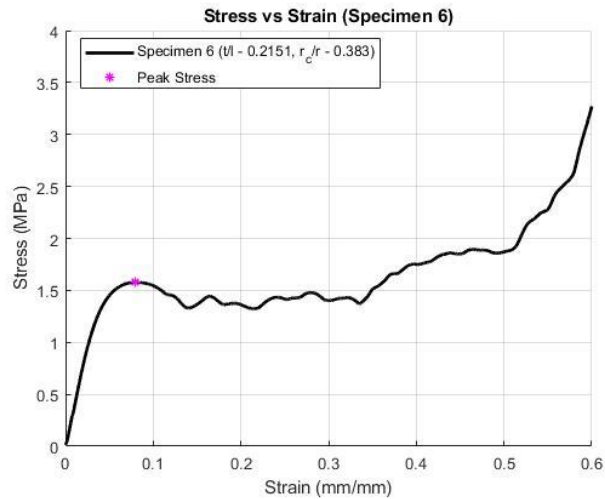


Figure 46: Comparing experimental data with numerical Von Mises stress contours, smooth plateau

In contrast, specimens with varying stress peaks (specimen 9 and baseline 2, Figure 47(a)&(b)) had increased stress concentration at the corner nodes leading to premature failure or fracture at the cell walls. Additionally, the stress peaks decreased for a slight increase in circularity from Baseline 2 to specimen 9 and similar t/l ratios. Therefore, it is hypothesized that the local stiffness characteristics at the corner node interface determine the honeycomb's failure behavior with plateau borders.

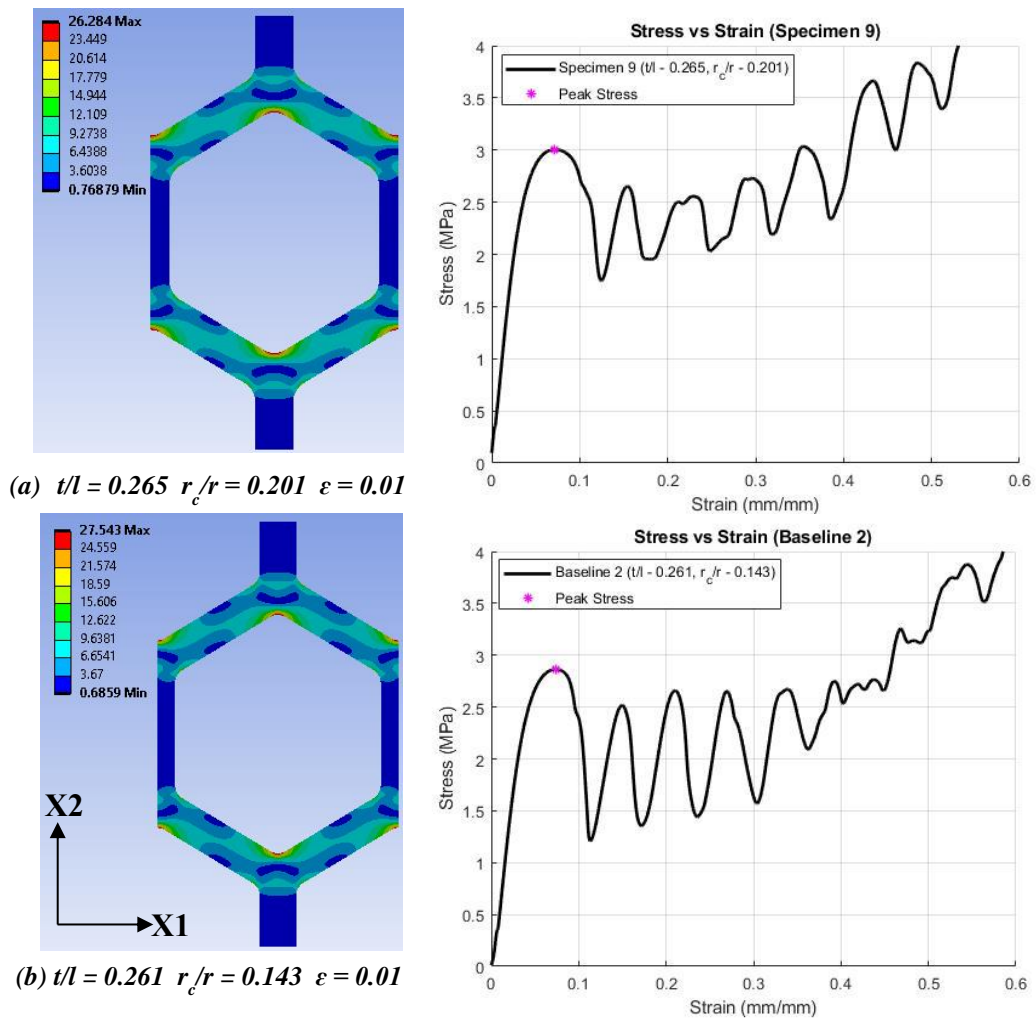
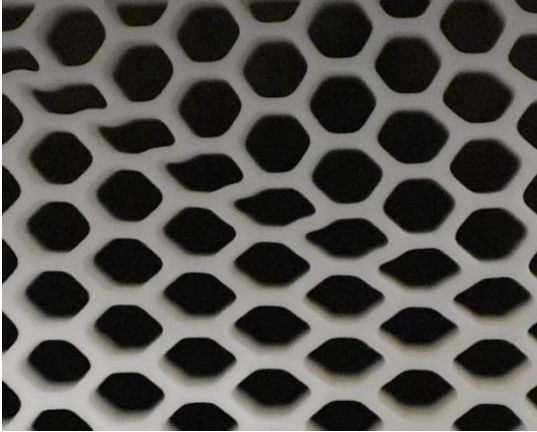


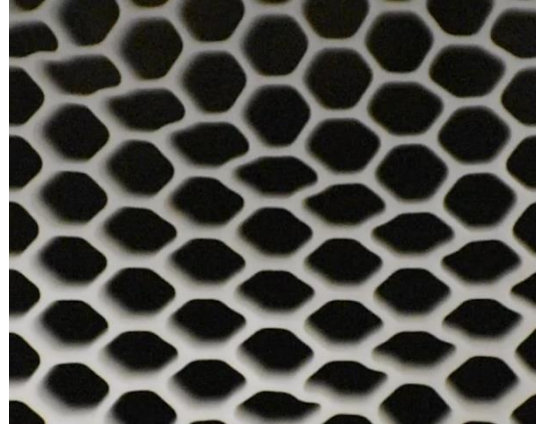
Figure 47: Comparing experimental data with Von Mises stress contours, rough plateau

$$t/l = 0.357 \quad r_c/r = 0.598$$



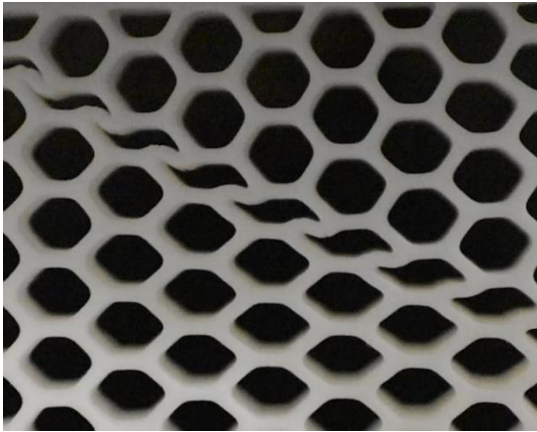
$$\varepsilon = 0.115$$

$$t/l = 0.21 \quad r_c/r = 0.589$$

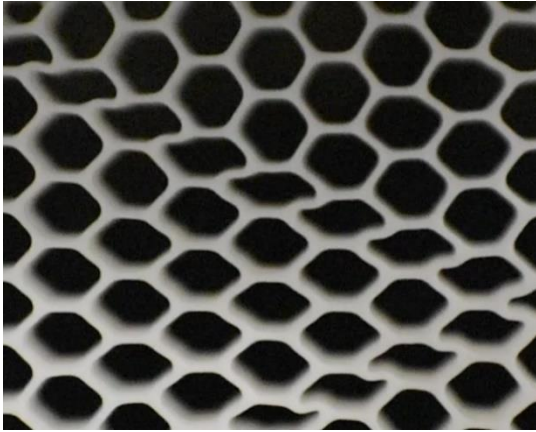


$$\varepsilon = 0.115$$

(a)

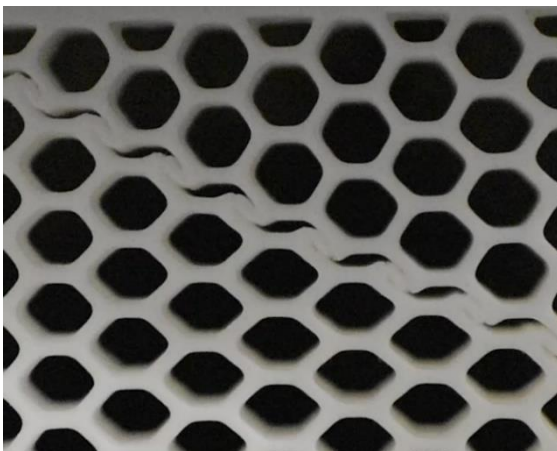


$$\varepsilon = 0.125$$



$$\varepsilon = 0.13$$

(b)



$$\varepsilon = 0.134$$



$$\varepsilon = 0.14$$

(c)

Figure 48: Rotational stiffness vs. Bending stiffness

The transition behavior between extensive plastic yielding and cell wall collapse of honeycombs with plateau borders is explained by still images comparing honeycombs with similar circularity and varying thicknesses at different strain levels (Figure 48). Initially, both the specimens start to deform with cell wall bending (Figure 48(a)). Still, at increased strain values, the specimen with the higher wall thickness begins to fail near the start point of the corner radii (Figure 48(b)) and finally causing the cell to collapse. In contrast, the honeycombs with similar circularity and low wall thickness continued to yield plastically without breaks or cracks. The plausible explanation for this transition behavior is the balance between the bending stiffness of the cell beam and the rotational stiffness (rotational resistance when the beams are rotated about the triangular node - a shaded region in Figure 49). The rotational stiffness model of a honeycomb with plateau borders by Chuang et al. [21] showed that the variable thickness beams acted like a rotational spring. Hence, it is hypothesized that if the bending stiffness of the beams present in thick-walled honeycombs overcomes the rotational stiffness, the cells start to collapse due to the beam failure, as observed in the experimental and numerical studies.

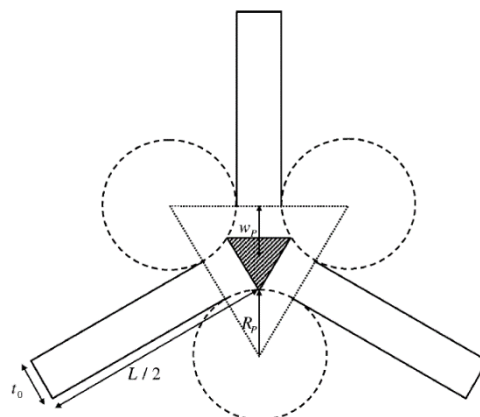


Figure 49: Honeycomb plateau border with triangular node

CHAPTER 6

CONCLUSION

This research aimed to conduct a quantitative analysis using experimental and numerical methods to characterize the hexagonal honeycombs' in-plane stress and stiffness behavior with a varying cell aspect ratio (t/l) and circularity (r_c/r). The local mechanical response is analyzed with a unit cell numerical model and variations in in-plane mechanical properties. Additionally, the experimental in-plane compression tests were conducted on 3D SLS printed honeycomb specimens to study the deformation behavior for honeycombs with different geometric parameters.

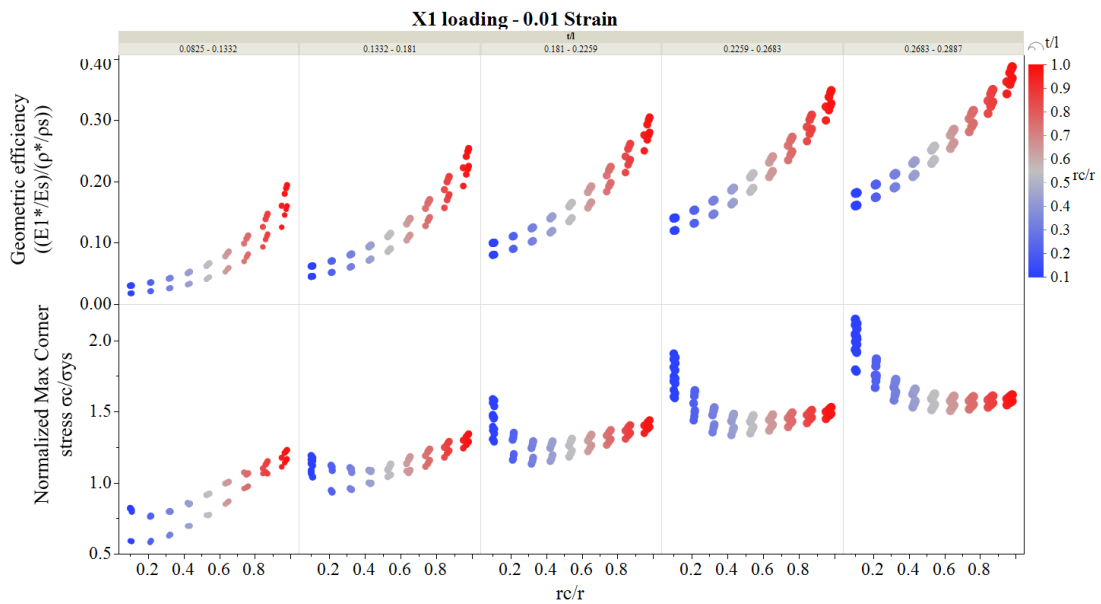


Figure 50: Summary of in-plane stress and stiffness characteristics

The parametric DOE study concluded that there is an optimum corner radius at different t/l ratios, which reduces stresses by delocalizing the stress maxima away from the corner nodes towards the start and endpoints of the corner radius arc. In addition, the corner radius was identified to improve the specific stiffness of the honeycomb. Still, the increase in t/l ratio was found to have a relatively higher contribution towards enhancing the stiffness characteristics. The general findings of the DOE study are summarized in Figure 50.

The experimental compression tests concluded that for an optimum combination of corner radius and wall thickness, the honeycomb specimens had a smooth stress-strain plateau and allowed the honeycombs to yield plastically with few breaks and fractures. In addition, thin-walled honeycombs with low circularities deformed similarly with a smooth stress-strain plateau to thick-walled honeycombs with high circularities, which conforms with the observations made in the parametric DOE study.

The comparative study between the experimental and numerical analysis hypothesized that the optimum combination of the t/l and r_c/r ratio corresponds to a mechanical balance between the bending stiffness of the cell wall beams and the rotational stiffness of the triangular node at the interface of the corner radius. Therefore, to maintain optimal performance (smooth plateau in stress-strain) of honeycomb structure under in-plane compression loading, the design parameters must ensure the aforementioned balance between cell wall bending and rotational stiffness in the presence of a corner radius.

6.1 Future work

In light of the structural benefits for regular honeycombs with a nodal curvature, it would be interesting to correlate the dependency of varying cell length ratio (t/l) and circularity (r_c/r) present in naturally occurring honeycombs. Figure 50 illustrates the different combinations of geometric features found in naturally occurring paper wasp honeycomb nests.

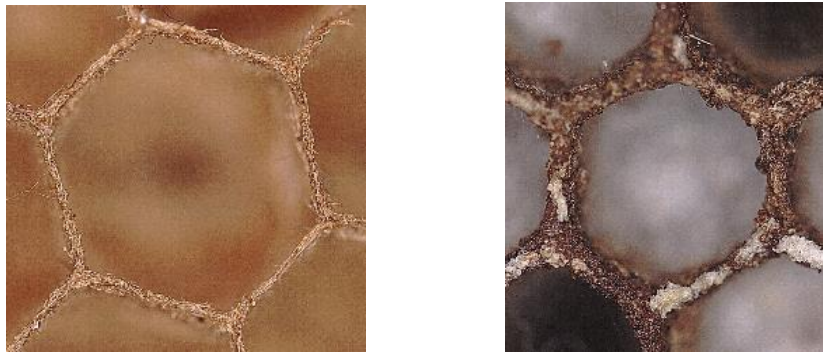


Figure 51: Paper wasp honeycomb nests (D. Goss)

In addition to the study conducted on 2D latticed honeycomb structures, there is an opportunity to explore the mechanical advantages of 3D latticed structures with a corner radius and varying beam morphology, as illustrated in Figure 51.

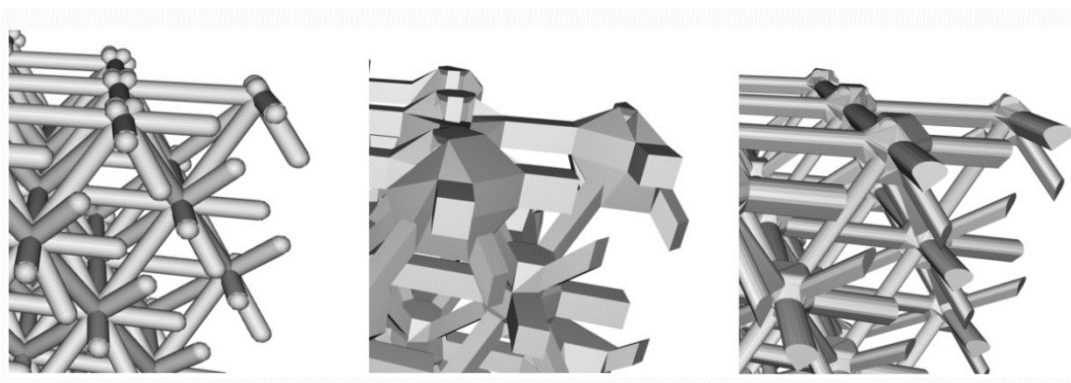


Figure 52: 3D lattice structures with varying beam morphologies

REFERENCES

- [1] Gibson, L. J., & Ashby, M. F. (1997). *Cellular Solids: Structure and Properties*. Cambridge University Press.
- [2] Zhang, Q., Yang, X., Li, P., Huang, G., Feng, S., Shen, C., Han, B., Zhang, X., Jin, F., Xu, F., & Lu, T. J. (2015). Bioinspired engineering of honeycomb structure – Using nature to inspire human innovation. *Progress in Materials Science*, 74, 332–400. <https://doi.org/10.1016/j.pmatsci.2015.05.001>
- [3] Bitzer, T. N. (2012). *Honeycomb technology: materials, design, manufacturing, applications, and testing*. Springer.
- [4] Baker, W. E., Togami, T. C., & Weydert, J. C. (1998). Static and dynamic properties of high-density metal honeycombs. *International Journal of Impact Engineering*, 21(3), 149–163.
- [5] Papka, S. D., & Kyriakides, S. (1994). In-plane compressive response and crushing of honeycomb. *Journal of the Mechanics and Physics of Solids*, 42(10), 1499–1532. [https://doi.org/10.1016/0022-5096\(94\)90085-x](https://doi.org/10.1016/0022-5096(94)90085-x)
- [6] Papka, S. D., & Kyriakides, S. (1998). Experiments and full-scale numerical simulations of in-plane crushing of a honeycomb. *Acta Materialia*, 46(8), 2765–2776. [https://doi.org/10.1016/s1359-6454\(97\)00453-9](https://doi.org/10.1016/s1359-6454(97)00453-9)
- [7] Habib, F. N., Iovenitti, P., Masood, S. H., & Nikzad, M. (2017). Cell geometry effect on in-plane energy absorption of periodic honeycomb structures. *The International Journal of Advanced Manufacturing Technology*, 94(5-8), 2369–2380. <https://doi.org/10.1007/s00170-017-1037-z>
- [8] Gibson, L. J. (2005). Biomechanics of cellular solids. *Journal of Biomechanics*, 38(3), 377–399. <https://doi.org/10.1016/j.jbiomech.2004.09.027>
- [9] Karihaloo, B. L., Zhang, K., & Wang, J. (2013). Honeybee combs: how the circular cells transform into rounded hexagons. *Journal of The Royal Society Interface*, 10(86), 20130299. <https://doi.org/10.1098/rsif.2013.0299>
- [10] Goss, D., Mistry, Y., Niverty, S., Noe, C., Santhanam, B., Ozturk, C., Penick, C. A., Lee, C., Chawla, N., Grishin, A., Shyam, V., & Bhate, D. (2020). Bioinspired Honeycomb Core Design: An Experimental Study of the Role of Corner Radius, Coping and Interface. *Biomimetics*, 5(4), 59. <https://doi.org/10.3390/biomimetics5040059>

- [11] Chuang, C.-H., & Huang, J.-S. (2002). Elastic moduli and plastic collapse strength of hexagonal honeycombs with plateau borders. *International Journal of Mechanical Sciences*, 44(9), 1827–1844. [https://doi.org/10.1016/s0020-7403\(02\)00139-x](https://doi.org/10.1016/s0020-7403(02)00139-x)
- [12] Yang, M.-Y., & Huang, J.-S. (2004). Numerical analysis of the stiffness and strength of regular hexagonal honeycombs with plateau borders. *Composite Structures*, 64(1), 107–114. [https://doi.org/10.1016/s0263-8223\(03\)00218-6](https://doi.org/10.1016/s0263-8223(03)00218-6)
- [13] Malek, S., & Gibson, L. (2015). Effective elastic properties of periodic hexagonal honeycombs. *Mechanics of Materials*, 91, 226–240. <https://doi.org/10.1016/j.mechmat.2015.07.008>
- [14] Timoshenko, S. P., Goodier, J. N., & Abramson, H. N. (1970). Theory of Elasticity (3rd ed.). *Journal of Applied Mechanics*, 37(3), 888–888. <https://doi.org/10.1115/1.3408648>
- [15] Sorohan, Ş., Sandu, M., Sandu, A., & Constantinescu, D. M. (2016). Finite Element Models Used to Determine the Equivalent In-plane Properties of Honeycombs. *Materials Today: Proceedings*, 3(4), 1161–1166. <https://doi.org/10.1016/j.matpr.2016.03.013>
- [16] ANSYS. (2017, July 14). *PLANE183 Element settings*. PLANE183. https://www.mm.bme.hu/~gyebro/files/ans_help_v182/ans_elem/Hlp_E_PLANE183.htm
- [17] Simone, A. E., & Gibson, L. J. (1998). Effects of solid distribution on the stiffness and strength of metallic foams. *Acta Materialia*, 46(6), 2139–2150. [https://doi.org/10.1016/s1359-6454\(97\)00421-7](https://doi.org/10.1016/s1359-6454(97)00421-7)
- [18] Warren, W. E., & Kraynik, A. M. (1987). Foam mechanics: the linear elastic response of two-dimensional spatially periodic cellular materials. *Mechanics of Materials*, 6(1), 27–37. [https://doi.org/10.1016/0167-6636\(87\)90020-2](https://doi.org/10.1016/0167-6636(87)90020-2)
- [19] Berger, J. B., Wadley, H. N., & McMeeking, R. M. (2017). Mechanical metamaterials at the theoretical limit of isotropic elastic stiffness. *Nature*, 543(7646), 533–537. <https://doi.org/10.1038/nature21075>
- [20] International Standard ISO 13314 (2011). Mechanical testing of metals. Ductility testing. Compression test for porous and cellular metals. <https://doi.org/10.3403/30203544u>
- [21] *Guide to Selective Laser Sintering (SLS) 3D Printing*. Formlabs. (n.d.). <https://formlabs.com/blog/what-is-selective-laser-sintering/>.

- [22] Chuang, C.-H., & Huang, J.-S. (2002). Effects of solid distribution on the elastic buckling of honeycombs. *International Journal of Mechanical Sciences*, 44(7), 1429–1443. [https://doi.org/10.1016/s0020-7403\(02\)00039-5](https://doi.org/10.1016/s0020-7403(02)00039-5)
- [23] Test Method for Tensile Properties of Plastics. (n.d.). <https://doi.org/10.1520/d0638-08>
- [24] Stoia, D., Linul, E., & Marsavina, L. (2019). Influence of Manufacturing Parameters on Mechanical Properties of Porous Materials by Selective Laser Sintering. *Materials*, 12(6), 871. <https://doi.org/10.3390/ma12060871>
- [25] *Polymer Properties Database*. Strain Hardening. (n.d.). <https://polymerdatabase.com/polymer%20physics/Strain%20Hardening.html>.

APPENDIX A

NYLON 12 MATERIAL MODEL

A.1 Experimental setup

The tensile test (Figure 53) was conducted for a total of 15 SLS 3D printed Nylon 12 Dogbones as per ASTM standards [23], D638-14 Type 4. The specimens were tested at strain rates of 10^{-3} , 10^{-4} & 10^{-5} s^{-1} using the INSTRON 5985 universal testing machine retrofitted with the tensile testing package. The elongation in gauge length was evaluated using the video extensometer, calibrated before the start of each test.

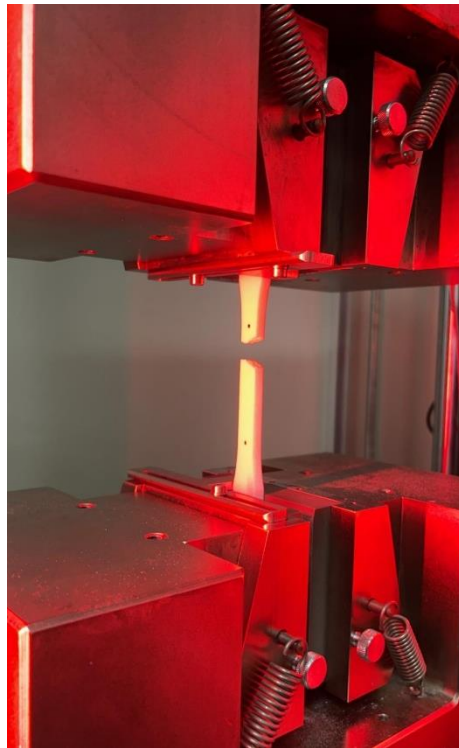


Figure 53: Nylon 12 tensile test setup

The force-displacement data is imported into Excel, and the true-stress strain curves were evaluated from the engineering stress-strain data and shown in Figure 54.

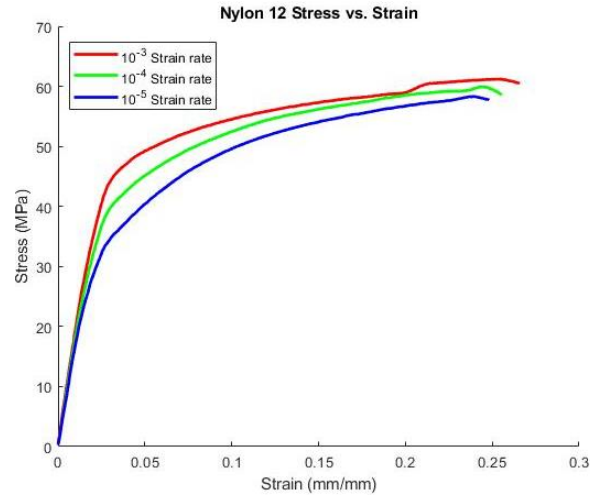


Figure 54: Nylon 12 True stress-strain plot at different strain rates

A.2 Material model numerical validation

The material data on strain rate of 10^{-5} s^{-1} was considered for the numerical study of the honeycombs, as the study was restricted to a static structural domain, and effects of visco-elasticity were neglected. The young modulus and yield stress of SLS 3D printed Nylon 12 properties determined experimentally was around 1720.374 MPa and 15.042 MPa. Through experimental studies, Stoia et al. [24] determined that the Poisson ratio of SLS 3D printed Nylon 12 dogbones to be around 0.408. The Multilinear Isotropic hardening model in ANSYS was used to define the plasticity behavior of the material above the yield limit (Figure 55).

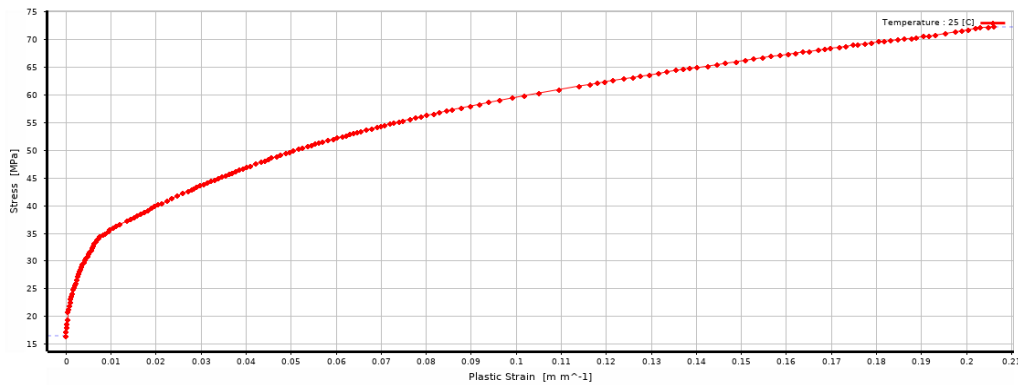
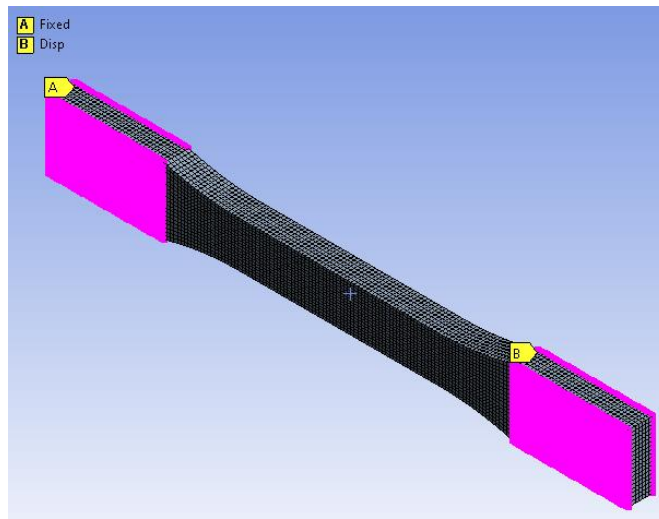
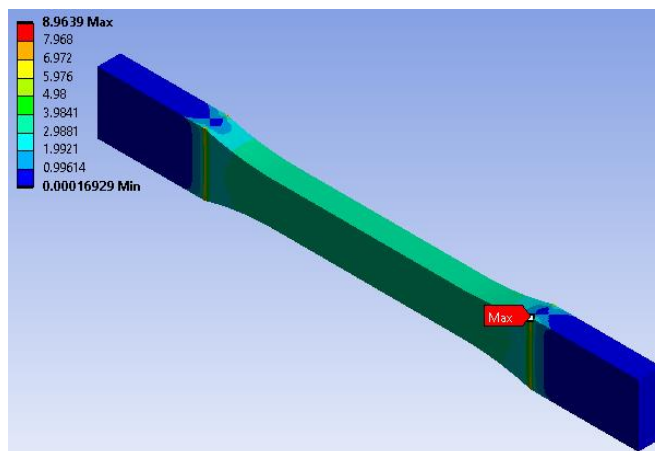


Figure 55: Multilinear Isotropic hardening plasticity model

A 3D Finite element analysis of a tensile test of a Nylon 12 dogbone was simulated in ANSYS to check the validity of the Nylon 12 material model. The dogbone meshed with 8-node brick elements, an element size of 1 mm, and large deformations were enabled (NLGEOM). A set of nodal displacement constraints was applied to the dogbone's grip sections, as illustrated in Figure 56(a). The von-mises equivalent strain evaluated at 0.9% is shown in Figure 56(b).



(a) Applied nodal boundary conditions



(b) Von-Mises Equivalent stress model ($\epsilon = 0.009$)

Figure 56: Nylon 12 Dogbone simulation

The force-displacement output from the simulation was compared with the experimental dataset for the strain rate at 10^{-5} s^{-1} (Figure 57). The simulation provided a stiffer output compared to experimental data. The deviation is potentially due to errors in dimensional accuracy and consistency of the dimension through the gauge section or due to the strain hardening assumption, which depends on the material's morphology (degree of crystallinity and branching) at the microscopic level [25]. In addition, an error in the Poisson's ratio assumption might also be a contributing factor. Another contributing factor could potentially be the large section thickness – the specimen was designed to have the largest thickness permissible in the standards, which may have contributed to corner stress heterogeneities.

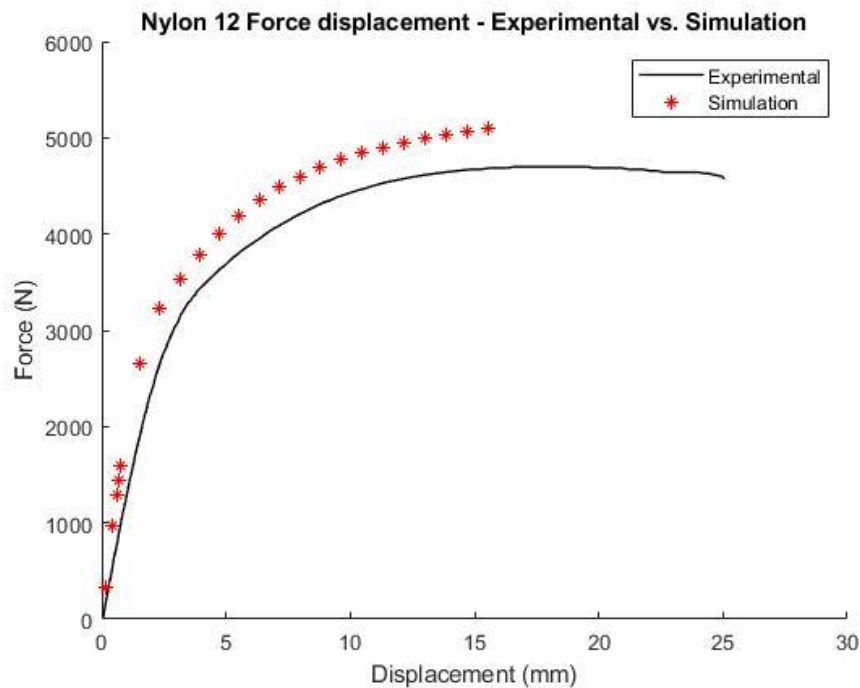


Figure 57: Force displacement comparison between experimental and numerical data

In addition to the force-displacement validation study, the variation in True stresses against the plastic strain was compared from both the experimental data and numerical study, as illustrated in Figure 58, and as expected, shows good agreement - the plastic behavior observed in the experimental true stress plots was able to be replicated in the numerical model. This suggests that the material model is suitable for numerical analysis.

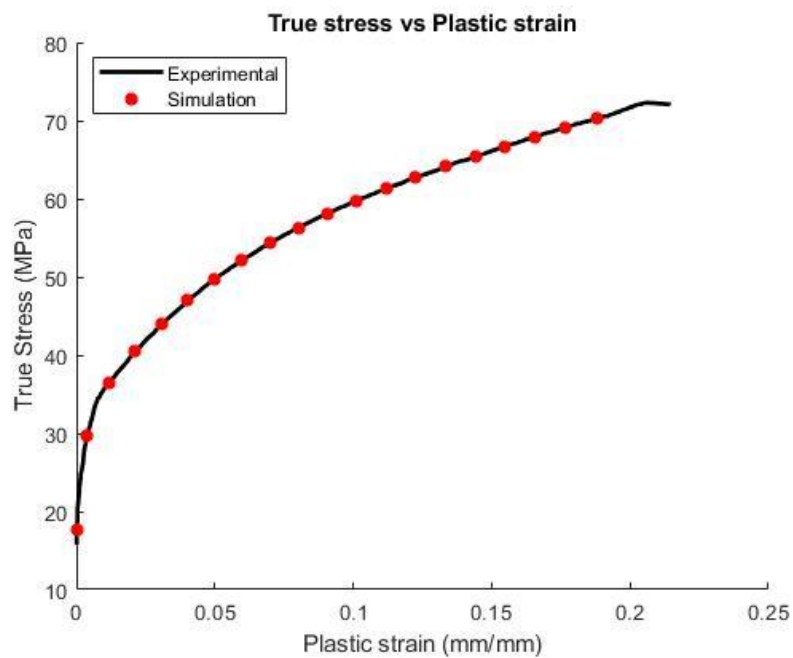


Figure 58: True stress and plastic strain comparison